Environmental and Experimental Botany 183 (2021) 104363

Contents lists available at ScienceDirect

Environmental and Experimental Botany

journal homepage: www.elsevier.com/locate/envexpbot

Impact of cadmium and zinc on proteins and cell wall-related gene expression in young stems of hemp (*Cannabis sativa* L.) and influence of exogenous silicon

Marie Luyckx [a], Jean-François Hausman [b], Arnaud Isenborghs [a], Gea Guerriero [b], Stanley Lutts [a,*]

[a] Groupe de Recherche en Physiologie végétale, Earth and Life Institute – Agronomy (ELI-A), Université catholique de Louvain, Louvain-la-Neuve, Belgium
[b] Environmental Research and Innovation (ERIN) Department, Luxembourg Institute of Science and Technology (LIST), Esch/Alzette, Luxembourg

ARTICLE INFO

Keywords:
Bast fiber
Cadmium
Cell wall
Fiber development
Heavy metals
Hemp
Mineral nutrition
Phytoremediation
Phytoextraction
Pollution
Remediation
Zinc

ABSTRACT

The study aims to determine the impact of Cd (20 μM) and Zn (100 μM) in the presence or absence of Si (2 mM) on plant development and fibre differentiation in young stem of hemp (*Cannabis sativa* L.). Gene expression and proteome involved in fibre development were analyzed. Both elements reduced the diameter of primary bast fibres. Cadmium negatively affected cellulose and lignin biosynthesis and decreased substitution of xylan in fibres, while Zn had an opposite impact on cellulose metabolism. Only a minor proportion of proteins were affected by both Cd and Zn, suggesting that the two heavy metals have a quite different impact on protein regulation in *C. sativa*. Si had a specific impact on some proteins observed in CdSi treatment comparatively to plants exposed to Cd in the absence of Si: 55 % of those proteins (10 among 18) were specifically regulated by this treatment and remained unaffected by Cd or Si applied alone. Six proteins were significantly regulated in ZnSi-exposed plants comparatively to Zn-treated ones and none of them was specifically regulated by Si in the absence of Zn. Diameter of bast fibre increased in response to Si in Cd-treated plants. This confirms that the presence of protecting Si confers a specific physiological status in relation to cell wall differentiation to heavy metal-treated plants.

1. Introduction

Human activities related to urbanization, industrialization and agriculture practices have resulted in the accumulation of heavy metals in soils and water in numerous areas of the world. Management of these contaminated sites constitutes a major environmental challenge since heavy metals may affect human health and environment stability. Conventional treatments for heavy metals removal from the soils include surface capping, soil flushing, air sparging, electrokinetic extraction, or vitrification, while chemical precipitation, coagulation, flocculation, and membrane filtration may be used to clean up contaminated water (Vareda et al., 2019). However, the use of plants to remove or stabilize pollutants has also been proposed as a promising alternative to those expensive remediation methods, but requires the availability of heavy metal-resistant species (Ali et al., 2013; Jaskulak et al., 2020).

Toxic effects of heavy metals on plants include alteration of mineral nutrition, photosynthesis modification in relation to reduced chlorophyll and carotenoid content, induction of oxidative stress or alteration of the plant water and hormonal status resulting in growth reduction and thus biomass production (Chandra and Kang 2016; Berni et al.,

Abbreviations: AAT, aspartate aminotransferase; AKR, probable aldo-keto reductase; BG, glucan endo-1_3-beta-glucosidase; CAD1, cinnamyl alcohol dehydrogenase 1-like; CAT, catalase; CBM3a, his-tagged recombinant protein recognizing crystalline cellulose; CES, cellulose synthase; CH5, class V chitinase-like; COMT, caffeic acid 3-*O*-methyltransferase; CW, cell wall; FLA, fasciclin-like arabinogalactan protein; GABA, γ-aminobutyrate; GAE6, UDP-glucuronate 4-epimerase 6; GDPDL3-like, glycerophosphodiester phosphodiesterase; GluDC, glutamate decarboxylase; GluDH, glutamate dehydrogenase; GSH, glutathione; LAC4, laccase 4; LM10, monoclonal antibody recognizing xylan; MET1, methyltransferase; MTHFR, methylenetetrahydrofolate reductase; NiR, nitrite reductase; P5CS, Δ-1-pyrroline-5-carboxylate synthase-like; PAE, pectin acetylesterase 3-like isoform X2; PC, phytochelatin; PCW, primary cell wall; PDF1, protodermal factor; PF, primary bast fibres; PME, pectinemethylesterase; PRX, peroxidase; RG-I, rhamnogalacturonan-I; RuBisCO, ribulose-1,5-bisphosphate carboxylase/oxygnase; SAMS, S-adenosylmethionine synthetase; SCW, secondary cell wall; SF, secondary bast fibres; SIR, sulfite reductase; SKU5, monocopper oxidase-like protein SKU5; SP, snap point; SuSy, sucrose synthase; TCA, tricarboxylic acid; UXS, UDP-glucuronic acid decarboxylase 6-like.

* Corresponding author.
E-mail address: stanley.lutts@uclouvain.be (S. Lutts).

https://doi.org/10.1016/j.envexpbot.2020.104363
Received 22 September 2020; Received in revised form 17 December 2020; Accepted 18 December 2020
Available online 2 January 2021

2018; Luyckx et al., 2019). Besides former industrial and mining areas which are frequently polluted by very high concentrations of toxic elements, agricultural soils may also be impacted by moderate pollution as a result of atmospheric contamination from surrounding areas and use of low quality fertilisers or pesticides. Since food crops cannot be cultivated in those areas as they represent a major risk for human health, non-food alternatives need to be proposed to producers (Pogrzeba et al., 2019; Feng et al., 2020).

Cannabis sativa L. is an annual high yielding industrial crop grown for its fibres and seeds (Morin-Crini et al., 2019; Pejic et al., 2009). As a multipurpose crop, *C. sativa* is receiving an increasing attention for the production of a wide range of bioactive molecules, but also as a source of feed in relation to the presence of oil, flour and protein and as a bioenergy crop (Andre et al., 2016; García-Tejero et al., 2019). Hemp can be used as potential crop for cleaning the soil from heavy metals (Citterio et al., 2003; Candilo et al., 2004; Angelova et al., 2004; Meers et al., 2005; Kumar et al., 2017) but could also be recommended as a good candidate for plant production on low contaminated substrates (Arru et al., 2004; Pietrini et al., 2019; Hussain et al., 2019a, 2019b). This implies that the non-edible parts of the plant need to be harvested and that hemp culture on marginal contaminated soil should focus on fibre cultivars (Linger et al., 2002), even if the seeds were recently reported to have a rather low metal content when plants were grown on slightly polluted substrates (Mihoc et al., 2012). Short hemp fibres, obtained as a waste from textile industry, can also be used as biosorbent for the removal of metal ions from polluted water (Vukcevic et al., 2014). Coating of harvested fibres with maltodextrin-1,2,3, 4-butanetetracarboxylic polymer was reported to provide ion-exchange properties improving heavy metal retention by a hemp-based felt (Loiacono et al., 2017). Besides such post-harvest treatments, heavy metals are also suspected to influence the pre-harvest development of hemp fibres, but data regarding the precise impact of element such as Cd and Zn on genes involved in this development in planta remain scant.

The stem of *Cannabis sativa* L. differentiate two types of fibres: (i) primary and secondary bast fibres associated with the conductive elements of phloem and bundles held together by pectins and lignin, and (ii) woody core fibres, called hurds or shivs, located in the xylem (Angelova et al., 2004; Behr, 2018; Guerriero et al., 2013; Morin-Crini et al., 2019). The hemp stem contains approximately 20–40 % of bast fibres and 60–80 % of hurds (Stevulova et al., 2014). The bast fibres initially elongate through intrusive growth, then cease elongation and start to thicken by secondary cell wall (SCW) deposition (Behr, 2018; Guerriero et al., 2017a). Plant fibre primary cell wall (PCW) consists mainly of cellulose, hemicelluloses and pectin (Pejic et al., 2009). They have the ability to bind heavy metal compounds (Vukcevic et al., 2014): metal ions indeed adsorb mainly to carboxylic (primarily present in hemicelluloses and pectin) and to some extent to hydroxylic (cellulose, hemicelluloses, and pectin) groups (Pejic et al., 2009; Hu et al., 2010; Vukcevic et al., 2014).

Secondary xylem, primary and secondary bast fibres undergo SCW deposition after the beginning of secondary growth (Behr, 2018). The composition of SCW is not similar for xylem- and phloem-located fibres. Xylem fibres differentiate a xylan-type SCW, while in the phloem fibres, SCW is of gelatinous (G-layer) type (Gorshkova et al., 2012). The CW of xylan-type fibres are lignified, contain predominantly xylan as hemicellulose constituent and show a typical layered structure (S1–S3) because of the different orientation of the cellulose microfibrils (Neutelings, 2011). The SCW of gelatinous fibres is also deposited in three layers, S1 and S2 compositions being similar to xylan-type wall while the G-layer has a very different organization: the major part of the G-layer is characterized by a high abundance of crystalline cellulose embedded in a rhamnogalacturonan-I (RG-I) matrix and a low content of xylan and lignin (Behr, 2018; Chernova et al., 2018; Guerriero et al., 2013, 2017a). The transition from bast fibre elongation via intrusive growth to SCW deposition occurs at a specific area called the "snap point" (SP) (Gorshkova et al., 2003). The formation of SCW in hemp phloem fibres begins with the deposition of the Gn-layer ("gelatinous-new") (Chernova et al., 2018). During further CW development, the Gn-layer is transformed to a "solid" G-layer: enzymatic digestion of the pectic matrix leads to the compaction of cellulose microfibrils and final organization of the G-layer (Chernova et al., 2018). It was also recently reported that in the young hemp hypocotyl, the G-layer has a loose structure (Gf) and that it gets compacted at later stages of development (Behr et al., 2019).

Guerriero et al. (2017a, b) and Behr et al. (2018) have higthlighted key genes coding for proteins involved in hemp fibre development, from bast fibre early growth stage (protodermal factor, PDF1), to SCW deposition (cellulose synthases *CESA4*, *CESA7*, *CESA8*), fasciclin-like arabinogalactan protein (*FLAs*), class III persoxidases; methyltransferase (*MET1*), S-adenosylmethionine synthetase (*SAMS*), including genes controlling the transition from elongation to thickening (acid phosphatase, AT1G04040). These molecular players are good candidates to evaluate the impact of heavy metal toxicity on plant fibre development. Besides transcriptomics, a proteomic analysis may also provide a useful set of information, but most of those analysis performed on *C. sativa* focused on cannabinoid synthesis rather than fibre CW formation (Aiello et al., 2016; Behr et al., 2018; Jenkins and Orsburn, 2020; Vincent et al., 2019). As far as exposure to heavy metal stress is concerned, data are only available for roots exposed to copper excess (Bona et al., 2007).

Any sustainable strategy helping the plant to cope with heavy metal toxicity could be usefully integrated in a phytomanagement scheme and this is especially the case for Si application (Wu et al., 2013; Adrees et al., 2015; Imtiaz et al., 2016; Etesami and Jeong, 2018; Bhat et al., 2019). Si is not considered essential for plant growth and development. However, increasing evidence in the literature show that this metalloid is beneficial to plants, especially under stress conditions (see Luyckx et al., 2017a for review). In hemp, the positive effects of Si on biomass production may be explained, among others, by an action on phytohormone balance regulating important stages of bast fibre development (Luyckx et al., 2017b). Si was recently shown to mitigate the impact of salt stress on hemp leaves (Berni et al., 2020). Guerriero et al. (2019) identified in hemp two NOD26-like intrinsic proteins exhibiting typical features reported to be associated with Si transport and revealed the presence of Si in isolated trichomes from the leaves, but also in the distal CW of bast fibres.

Silica hydrophobic coating is frequently used during processing of harvested fibres to reduce their water absorption (Jiang et al., 2018) or as a fire retardant (Branda et al., 2016). According to Hussain et al. (2019b), silica matrix used for composite with hemp shive may assume multifunctional purposes which suggest that Si may, to some extent, directly interact with hemp fibres. However, the impact of Si on hemp fibre during their development process remains poorly documented, especially in the case of heavy metal-exposed plants.

The present work was therefore undertaken in order to determine the impact of Cd and Zn in the presence or absence of Si on plant development and fibre differentiation in relation to heavy metal accumulation in young stem of *C. sativa*. The expression of genes regulating fibre development was analyzed and the proteome of hypocotyls was characterized.

2. Material and methods

2.1. Plant material and growing conditions

Seeds of a monoecious hemp fibre variety (*Cannabis sativa* cv. Santhica 27) were sown in loam substrate in greenhouse conditions. After one week, the obtained seedlings were transferred to nutrient Hoagland solution (in mM: 2.0 KNO_3, 1.7 $Ca(NO_3)_2$, 1.0 KH_2PO_4, 0.5 NH_4NO_3, 0.5 $MgSO_4$, and in μM: 17.8 Na_2SO_4, 11.3 H_3BO_3, 1.6 $MnSO_4$, 1 $ZnSO_4$, 0.3 $CuSO_4$, 0.03 $(NH_4)_6Mo_7O_{24}$ and 14.5 Fe-EDDHA) in 25 L tanks. For each tank, 10 seedlings were adapted to plugged holes in a polystyrene plate floating at the top of the solution. Tanks (24) were

placed in a phytotron under fully controlled environmental conditions (permanent temperature of 24 ± 1 °C with a mean light intensity of 230 μmoles $m^{-2}s^{-1}$ provided by Phillips lamps (Philips Lighting S.A., Brussels, Belgium) (HPI-T 400 W), with a photoperiod of 16 h under a relative humidity of 65 %).

After one week, half of the tanks received Si in the form of H_2SiO_3 to a final concentration of 2 mM Si. Metasilicic acid was obtained from a pentahydrate sodium metasilicate (Na_2SiO_3 x 5 H_2O) which was passed through an H^+ ion exchanger resin IR 20 Amberlite type according to Dufey et al. (2014). Tanks were randomly arranged in the phytotron and nutrient solution was permanently aerated by SuperFish Air Flow 4 pump. After an additional week of acclimatization, heavy metals were applied in the form of $CdCl_2$ (final concentration of 20 μM) and $ZnCl_2$ (100 μM) as previously stated (Luyckx et al., 2017b). The pH of the solution was maintained at 5.5. Solubility of added heavy metals was confirmed by the Visual MINTEQ09 software. Six treatments were thus defined, considering the presence of heavy metals and the concomitant presence or absence of Si and will be designed as C (control: no heavy metals and no Si), CSi, Cd, CdSi, Zn and ZnSi (4 tanks per treatment). Plants were harvested after one week of treatment and roots were thoroughly rinsed in deionized water: 4 plants per tank were selected to measure stem length and diameter, number of leaves, root length, fresh and dry weight (obtained after 72 h of incubation in an oven at 70 °C) and heavy metal concentration in roots, leaves and stems. The remaining plants from the same tank were pooled: roots, leaves and stems were separated. Hypocotyl parts of the stem were separated from epicotyls, frozen in liquid nitrogen and then stored at −80 °C until subsequent transcriptomic and proteomic analysis. Segments of stem in the internode containing the SP were rapidly excised for confocal microscope observation.

2.2. Mineral concentration

Plant samples were dried at 70 °C for 72 h. For Cd and Zn quantification, 50−100 mg dry material (DM) were then digested in 68 % HNO_3 and acid evaporated to dryness on a sand bath at 80 °C. Minerals were incubated with a mix of HCl 37 %-HNO_3 68 % (3:1) and the mixture was slightly evaporated, dissolved in distilled water and filtrated on Whatman n°2 filter papers. For Si quantification, 1 g DM were placed in an oven and heated to 500 °C for 48 h. Ashes were then mixed with 0.4 g tetraborate and 1.6 g metaborate and heated to 1000 °C for 5 min. The obtained pellet was dissolved with 25 % HNO_3. Cations were quantified by Inductively Coupled Plasma-Optical Emission Spectroscopy (Varian, type MPX).

2.3. Gene expression analysis

Total RNA was extracted from hypocotyls according to Guerriero et al. (2017a) and Mangeot-Peter et al. (2016) using the RNeasy Plant Mini Kit (Qiagen) treated on-column with DNase I. The RNA concentration and quality were measured for each sample by using a Nanodrop ND-1000 (Thermo Scientific) and a 2100 Bioalyzer (Agilent Life Sciences), respectively. The RNA integrity number (RIN) of all samples was higher than 7, and the ratios A260/280 and A260/230 were between 1.7 and 2.4. The extracted RNA was retrotranscribed into cDNA using the SuperScript II reverse transcriptase (Invitrogen) and random primers, according to the manufacturer's instructions. The synthesized cDNA was diluted to 2 ng/μL and used for the RT-qPCR analysis in 384-well plates. An automated liquid handling robot (epMotion 5073, Eppendorf) was used to prepare the 384-well plates. To check the specificity of the amplified products, a melt curve analysis was performed. The relative gene expression was calculated with qBase^{PLUS} (version 2.5, Biogazelle) by using the reference genes (*eTIF4E*, *TIP41*, *F-box* and *RAN*, Mangeot-Peter et al., 2016). Statistics (ANOVA2) were performed using R (version 3.3.1).

The target genes were chosen on the basis of preliminary results (Guerriero et al., 2017a, 2017b) and belong to genes regulating the lignification process [methyltransferase (*MET1*), S-adenosylmethionine synthase (SAMS), class-III peroxidases (*PRX49, PRX 52, PRX 72*), genes coding for SCW cellulose synthases (*CesA4, CesA7, CesA8*) and fasciclin-like arabinogalactan protein (*FLA3, FLA11, FLA13, FLA19*).

The corresponding primers were designed using Primer3Plus (http://www.bioinformatics.nl/cgi-bin/primer3plus/primer3plus.cgi/) and verified with the OligoAnalyzer 3.1 tool (Integrated DNA technologies, http://eu.idtdna.com/calc/analyzer). Primer efficiencies were checked via qPCR using 6 serial dilutions of cDNA (10, 2, 0.4, 0.08, 0.016, 0.0032 ng/μL). For each considered gene, selected primers are listed in Table S1.

2.4. Proteomic analysis

For each sample, 500 mg fresh material (FM) of *C. sativa* hypocotyl were homogenized in a Potter (Wheaton) homogenizer in 2 mL of homogenization buffer (50 mM Tris, pH 7.5 (HCl), 2 mM EDTA, 5 mM dithiothreitol (DTT), protease inhibitor mix (1 mM phenylmethylsulfonyl fluoride (PMSF), 2 μg/mL each of leupeptin, aprotinin, antipain, pepstatin, and chymostatin), 0.6 % w/v polyvinylpolypyrrolidone, 30 mM spermine) and the homogenate centrifuged for 5 min at 2000 rpm and 4 °C. Protein extracts were centrifuged at 2 °C for 30 min at 54,000 rpms (TLA55, Optima-Beckman-Coulter) to obtain a pellet of crude membranes and supernatant.

Twenty μg of each sample were transferred to 0.5 mL polypropylene Protein LoBind Eppendorf tubes and precipitated with chloroform-methanol method (Wessel and Flügge, 1984); 20 μL of 100 mM TEAB (triethylammonium bicarbonate) were then added to reach pH 8.5. Proteins were reduced by 5 mM DTT (dithiothreitol) and alkylated by 15 mM iodoacetamide. Proteolysis was performed with 0.5 μg of trypsin and allowed to continue overnight at 37 °C. Each sample was dried under vacuum with Savant Speed Vac Concentrator.

Before peptide separation, the samples were dissolved in 20 μL of 0.1 % (v/v) formic acid and 2 % (v/v) acetonitrile (ACN). Peptide mixture was separated by reverse phase chromatography on a NanoACQUITY UPLC MClass system (Waters) working with MassLynx V4.1 (Waters) software; 200 ng of digested proteins were injected on a trap C18, 100 Å 5 μm, 180 mm x 20 mm column (Waters) and desalted using isocratic conditions with at a flow rate of 15 μL/min using a 99 % formic acid and 1 % (v/v) ACN buffer for 3 min. The peptide mixture was subjected to reverse phase chromatography on a C18, 100 Å 1.8 mm, 75 μm x 150 mm column (Waters) PepMap for 120 min at 35 °C at a flow rate of 300 nL/min using a two part linear gradient from 1 % (v/v) ACN, 0.1 % formic acid to 35 % (v/v) ACN, 0.1 % formic acid and from 35 % (v/v) ACN, 0.1 % formic acid to 85 % (v/v) ACN, 0.1 % formic acid. The column was re-equilibrated at initial conditions after washing 10 min at 85 % (v/v) ACN, 0.1 % formic acid at a flow rate of 300 nL/min. For online LC–MS analysis, the nanoUPLC was coupled to the mass spectrometer through a nano-electrospray ionization (nanoESI) source emitter.

IMS-HDMSE (Ion Mobilty Separation-High Definition Enhanced) analysis was performed on an SYNAPT G2-Si high definition mass spectrometer (Waters) equipped with a NanoLockSpray dual electrospray ion source (Waters). Precut fused silica PicoTipR Emitters for nanoelectrospray, outer diameters: 360 μm; inner diameter: 20 μm; 10 μm tip; 2.5" length (Waters) were used for samples and Precut fused silica TicoTipR Emitters for nanoelectrospray, outer diameters: 360 μm; inner diameter: 20 mm; 2.5" length (Waters) were used for the lock mass.solution. The eluent was sprayed at a spray voltage of 2.4 kV with a sampling cone voltage of 25 V and a source offset of 30 V. The source temperature was set to 80 °C. HDMSE method in resolution mode was used to collect data from 15 min after injection to 106 min. This method acquires MSE in positive and resolution mode over the *m/z* range from 50 to 2000 with a scan time of 1 s. with a collision energy ramp starting from ion mobility bin 20 (20 eV) to 110 (45 eV). The collision energy in

the transfer cell for low-energy MS mode was set to 4 eV. For the post-acquisition lock mass correction of the data in the MS method, the doubly charged monoisotopic ion of [Glu1]-fibrinopeptide B was used at 100 fmol/mL using the reference sprayer of the nanoESI source with a frequency of 30 s at 0.5 mL/min into the mass spectrometer.

HDMSE data were processed with Progenesis QI (Nonlinear DYNAMICS, Waters) software using *C. sativa* NCBI database downloaded october 8, 2019. Carbamidomethylation as the fixed cysteine modification, oxidation as the variable methionine modification, trypsin as the digestion enzyme were selected and one miscleavage allowed.

2.5. Confocal microscope observation

Segments of stem tissue in the internode containing the SP were rapidly excised from fresh plants with a scalpel and dipped into tissue freezing media (O.C.T., Tissue Tek, Jung etc.), and into propane cooled by liquid nitrogen. The plant pieces were next sectioned at 60 µm thickness with a Leica CM3050 cryotome (Leica), placed in Al holders and transferred to an Alpha 2–4 Christ freeze dryer (−50 °C, 0.04 mbar, 3 days). Freeze-dried cross-sections were photographed using a digital camera (AxioCam) mounted on a Zeiss Axioscope 2 fluorescence microscope (wavelenght: 405 nm).

2.6. Immunohistochemistry

Hemp stems sections of 5 mm in the internode containing the SP were fixed in FAA (90 mL ethanol 70 %/5 mL glacial acetic acid/5 mL formaldehyde 35 %) for 24 h at room temperature, dehydrated in ethanol series (70 %–80 %-100 %) and ethanol:butanol series (2/3:1/3–1/3:2/3 – butanol 100 %), impregnated in paraffin 12 h at 37 °C and 24 h at 60 °C, and finally included. The plant pieces were next sectioned at 10 µm thickness with a microtome (Leica), and used for immunohistochemistry (IHC). Image acquisition was performed with a confocal microscope LSM 710 (Zeiss).

The protocol used for immunohistochemistry is described by Behr et al. (2016): LM10 (xylan, Plant Probes) antibody was diluted 10-fold in milk protein (MP)/PBS (5 % w/v). Sections were then incubated for 1.5 h, rinsed three times in PBS and incubated for 1.5 h with the anti-rat IgG coupled to FITC (Sigma) diluted 100-fold in MP/PBS. Before observation, three washings with PBS were performed. CBM3a (crystalline cellulose, Plant Probes) was diluted to 10 µg/mL in MP/PBS, incubated in mouse anti-His monoclonal antibody (1 % in MP/PBS, Sigma) and finally incubated in 50-fold diluted anti-mouse IgG coupled to FITC (Sigma). Each incubation lasted for 1.5 h. Between each step, three washes with PBS were performed. The slides were observed with the following settings: excitation at 488 nm, filter HFT 493/564 and emission recorded with LP 505. The microscope settings were kept rigorously constant between the different observations for a given epitope. Negative controls where either the primary or secondary antibody was omitted resulted in a very weak and negligible signal.

Images were imported into ImageJ to get quantitative data and were calibrated with the "Set Scale" command. Fluorescence intensity in the different stem tissues was measured using the "Freehand selections" command the, and the "Straight line" was used to measure both the diameter and the CW thickness of bast fibres (primary and secondary bast fibres). Three plants per treatment were analyzed and 6–10 measurements were made for each one.

2.7. Statistical analysis

Four independent biological replicates and three technical replicates were analyzed for each condition. Normality of the data was verified using Shapiro-Wilk tests and the data were transformed when required. Homogeneity of the data was verified using Levene's tests. ANOVA 2 were performed at a significant level of p-value <0.05 using R (version 3.3.1) considering the type of heavy metal treatment, and the Si application as main factors. Means were compared using Tukey's HSD all-pairwise comparisons at 5 % level as a post-hoc test.

For proteomic analysis, non-conflicting method was used as relative quantification method. To identify statistically significant differentially expressed proteins, combined criteria of a minimum of three or greater unique peptides, a two-fold change ratio or greater and a p-value <0.05 in the Student's t-tests were adopted.

3. Results

3.1. Impact of Cd and Zn on plant physiological parameters

Phenotypes of plant cultivated in the different conditions are illustrated in Fig. S1. In the absence of heavy metals, Si had no impact on root and stem length, stem diameter and total leaf number (Table 1). In contrast, both Cd and Zn in the absence of H_2SiO_3 significantly reduced root length, stem diameter and total leaf number while only Cd had a significant impact on stem length. The application of 2 mM H_2SiO_3 tended to slightly mitigate the deleterious impact of heavy metal stress on root length and stem diameter, although no significant difference was recorded for the mean values. Heavy metals also significantly reduced root, stem and leaf dry weight (DW) (Table 2), Cd being more toxic than Zn for root and leaves. Heavy metals reduced the water content in stems, only. Si tended to slightly increase the mean DW of roots in Cd-treated plants and of both stem and leaves in Zn-treated ones, although the difference was not significant considering the high variability occurring among replicates.

3.2. Mineral content

Cd (Table 3) was detected in Cd- and CdSi-treated plants only (detection limit: 0.013 mg/L). The root Cd concentration was significantly higher than in leaves (p-values < 0.01) while the stem showed an intermediate value. H_2SiO_3 application slightly decreased Cd content in roots and stems. Zn excess strongly increased root, stem and leaf Zn concentration (Table 3), with higher values in roots than in stems and leaves (p-value < 0.01). Exposure to H_2SiO_3 increased root and leaf Si concentration in the absence and in the presence of heavy metals but the recorded increase in Si was not significant in the stem (Table 3). Si concentration was higher in the roots and leaves of ZnSi treated plants than in those of CdSi-treated ones while an opposite trend was recorded for the stem.

3.3. Gene expression in the stem

The hierarchical clustering of the expression profiles (represented as a heatmap; Fig. 1) for the various treatments was performed using a Euclidean distance matrix in complete linkage. The clustering resulted in a separation between control plants (C, CSi), Cd exposed plants (Cd,

Table 1
Root length, stem length and diameter, and total leaf number of *Cannabis sativa* (cv. Santhica 27) exposed for one week to Cd (20 µM) or Zn (100 µM), in the presence or in the absence of 2 mM H_2SiO_3. Data are means ± standard errors (n = 4). Values with different letters are significantly different (P < 0.05; Tukey's HSD all-pairwise comparisons).

Treatment	Root length (cm)	Stem length (cm)	Stem diameter (mm)	Total leaf number
C	42.60 ± 2.21 *b*	27.12 ± 5.91 *b*	7.13 ± 0.77 *c*	10.20 ± 0.45 *b*
CSi	40.92 ± 8.49 *b*	29.78 ± 7.49 *b*	6.68 ± 0.50 *bc*	10.20 ± 0.45 *b*
Cd	31.22 ± 3.99 *a*	12.66 ± 2.64 *a*	4.58 ± 0.48 *a*	7.80 ± 0.84 *a*
CdSi	36.18 ± 3.26 *ab*	14.90 ± 4.79 *a*	5.16 ± 0.52 *ab*	8.40 ± 0.55 *a*
Zn	30.10 ± 5.96 *a*	20.20 ± 4.37 *ab*	4.65 ± 1.05 *a*	9.40 ± 1.14 *a*
ZnSi	34.20 ± 1.09 *ab*	21.78 ± 2.68 *ab*	4.97 ± 1.20 *a*	9.20 ± 0.84 *a*

Table 2
Roots, stems and leaves dry weight and water content of *Cannabis sativa* (cv. Santhica 27) exposed for one week to Cd (20 μM) or Zn (100 μM), in the presence or in the absence of 2 mM H_2SiO_3. Data are means ± standard errors ($n = 4$). Values with different letters are significantly different ($P < 0.05$; Tukey's HSD all-pairwise comparisons).

Treatment	Dry weigth (g)			Water content (%)		
	Roots	Stems	Leaves	Roots	Stems	Leaves
C	8.80 ± 1.04 *c*	7.90 ± 0.30 *b*	18.07 ± 1.62 *b*	93 ± 1.3 *a*	92 ± 1.3 *b*	86 ± 2.1 *a*
CSi	7.93 ± 0.50 *c*	6.77 ± 1.18 *b*	14.73 ± 3.85 *b*	93 ± 1.1 *a*	92 ± 0.4 *b*	82 ± 1.2 *a*
Cd	3.07 ± 1.51 *a*	2.23 ± 1.02 *a*	3.33 ± 0.71 *a*	93 ± 1.1 *a*	89 ± 1.6 *a*	81 ± 5.5 *a*
CdSi	3.87 ± 0.76 *ab*	2.10 ± 0.62 *a*	3.60 ± 0.26 *a*	92 ± 3.0 *a*	82 ± 1.6 *a*	86 ± 13.1 *a*
Zn	3.97 ± 1.27 *b*	2.87 ± 1.19 *a*	6.20 ± 2.51 *c*	92 ± 1.1 *a*	77 ± 7.9 *a*	79 ± 5.2 *a*
ZnSi	3.77 ± 1.47 *ab*	3.67 ± 1.53 *a*	8.07 ± 3.71 ac	91 ± 1.1 *a*	86 ± 2.1 *a*	78 ± 1.9 *a*

Table 3
Cadmium, zinc and silicon concentration (in mg kg^{-1} DW) in roots, stems and leaves of *Cannabis sativa* (cv Santhica 27) exposed for one week to Cd (20 μM) or Zn (100 μM), in the presence or in the absence of 2 mM H_2SiO_3. Data are means ± standard errors ($n = 4$). For each organ and element, values with different letters are significantly different at $P < 0.05$ according to the Tukey's HSD all-pairwise comparisons (nd = not detected).

		Treatment					
		C	CSi	Cd	CdSi	Zn	ZnSi
Cd (mg kg^{-1} DW)	Roots	nd	nd	2441 ± 151 *a*	1910 ± 759 *a*	nd	nd
	Stems	nd	nd	1246 ± 439 *a*	1036 ± 42 *a*	nd	nd
	Leaves	nd	nd	689 ± 49 *a*	753 ± 155 *a*	nd	nd
Zn (mg kg^{-1} DW)	Roots	259 ± 25 *a*	255 ± 143 *a*	388 ± 102 *a*	292 ± 100 *a*	7518 ± 1422 *b*	5458 ± 2511 *b*
	Stems	52 ± 14 *a*	38 ± 2 *a*	111 ± 25 *a*	103 ± 13 *a*	1169 ± 225 *b*	1393 ± 438 *b*
	Leaves	59 ± 5 *a*	63 ± 6 *a*	42 ± 13 *a*	40 ± 8 *a*	1185 ± 275 *b*	994 ± 221 b
Si (mg kg^{-1} DW)	Roots	220 ± 36 a	2030 ± 240 *b*	236 ± 63 *a*	1598 ± 147 *b*	225 ± 49 a	6854 ± 578 *c*
	Stems	98 ± 27 *ab*	160 ± 4 *b*	nd	83 ± 31 *a*	48 ± 3 *b*	129 ± 19 *ab*
	Leaves	47 ± 3 *c*	3297 ± 1223 *b*	49 ± 2 *c*	5691 ± 2098 *a*	63 ± 23 *c*	2210 ± 287 *b*

CdSi) and Zn exposed plants (Zn, ZnSi). In plants that were not exposed to heavy metals, exposure to Si stimulated the expression of CesA4, CesA8, FLA11, and MET1, the difference being significant for CesA4, only.

In Cd-stressed plants, several transcripts related to SCW formation were less abundant as compared to the control, notably *CesA7, CesA8, FLA3, FLA11, FLA13*, and *FLA19* involved in cellulose deposition (Behr et al., 2016; Guerriero et al., 2017b). In the same plant samples, somes genes controlling several biochemical pathways, including the regulation of lignification, displayed a different expression pattern: MET1 and SAMS (generation of methyl donors) were down-regulated by Cd, whereas *PRX49*, *PRX52* and *PRX72* (genes controlling lignification; Herrero et al. (2013) and previously shown to be upregulated in hypocotyls aged 15 and 20 days; Behr (2018) were more expressed in Cd-treated plants than in controls. No significant effect of Si application on the expression of genes in Cd-stressed plants was detected but, once again, trends may be observed: PDF1, a gene shown to be upregulated in the young hemp internode (Guerriero et al., 2017a) and maybe involved in fibre initation, *CesA4, FLA13, FLA19, FLA3, MET1, PRX49, PRX52* seem to be more expressed in CdSi-treated plants than in Cd exposed ones, while a gene encoding an acid phosphatase influencing CW-related processes in bast fibres during the transition from elongation to thickening (Guerriero et al., 2017a), *SAMS* and *PRX72* showed an inverse trend.

In Zn-treated plants, *CesA4, FLA19, PRX49, PRX52* and the gene coding for the acid phosphatase were upregulated compared to control plants. A higher expression of *PDF1*, *CesA8* and *CesA7* was observed in Zn-treated plants when exposed to Si comparatively to Zn-treated plants cultivated in the absence of Si. The abundance of transcripts coding for the acid phosphatase, PDF1, FLA19, CESA7 and PRX49 were higher in ZnSi-treated plants than in those exposed to Si in the absence of heavy metals (CSi).

3.4. Proteomics

The data relative to the impact of the treatments on protein regulation are provided in Table 4 which simultaneously considers soluble and membrane-bound protein fractions.

Hemp response to Cd resulted in a significant increase in the abundance of 2 proteins involved in tricarboxylic acid (TCA) pathway, one controlling callose remodelling (glucan endo-1_3-beta-glucosidase, BG), one protein regulating lignin biosynthesis (cytochrome P450 CYP73A100-like, CYP73A100), a protein regulating proline biosynthesis (Δ-1-pyrroline-5-carboxylate synthase-like, P5CS), a protein responsible for glutamate metabolism (glutamate dehydrogenase, GluDH), a protein involved in sulphate assimilation (sulfite reductase, SIR), 3 protein involved in protein synthesis and 3 involved in proteolysis, 3 proteins controlling transport, 4 involved in ionic homeostasis, a protein managing cell organization, 4 proteins involved in signal transduction and metabolism regulation and 5 in cell rescue. Conversely, Cd treatment negatively impacted the abundance of a protein involved in photosynthesis (ribulose-1,5-bisphosphate carboxylase/oxygnase, RuBisCO small subunit), 2 proteins regulating carbohydrate metabolism, one in TCA cycle, one protein involved in fermentation, a protein controlling γ-aminobutyrate (GABA) shunt, proteins controlling cellulose biosynthesis (sucrose synthase, SuSy; cellulose synthase; CESA7, CESA8), lignin biosynthesis (caffeic acid 3-O-methyltransferase, COMT; laccase 4, LAC4; CYP736A12), lignin monomer methylation (methylenetetrahydrofolate reductase, MTHFR) and pectin synthesis (UDP-glucuronate 4-epimerase 6, GAE6), 2 proteins involved in amino acid metabolism, 6 proteins regulating protein synthesis and one involved in protein folding, 2 proteins involved in transport, 4 proteins managing cellular organization, 6 proteins involved in signal transduction and metabolism regulation and a protein controlling cell rescue (class V chitinase-like, CH5) (Table 4). Cd had no direct impact on proteins regulating cell division but it nevertheless affected the cytoskeleton through a decrease in tubulin alpha-1 chain. As shown in Fig. 2, the most important category of proteins up-regulated by Cd was related to cell rescue and defence and includes protein dealing with oxidative stress such as catalase and peroxidases. Conversely, most down-regulated proteins were related to SCW synthesis, as it was the case for cellulose synthase CESA7 and CESA8 or for caffeic acid 3-*O*-methltransferase

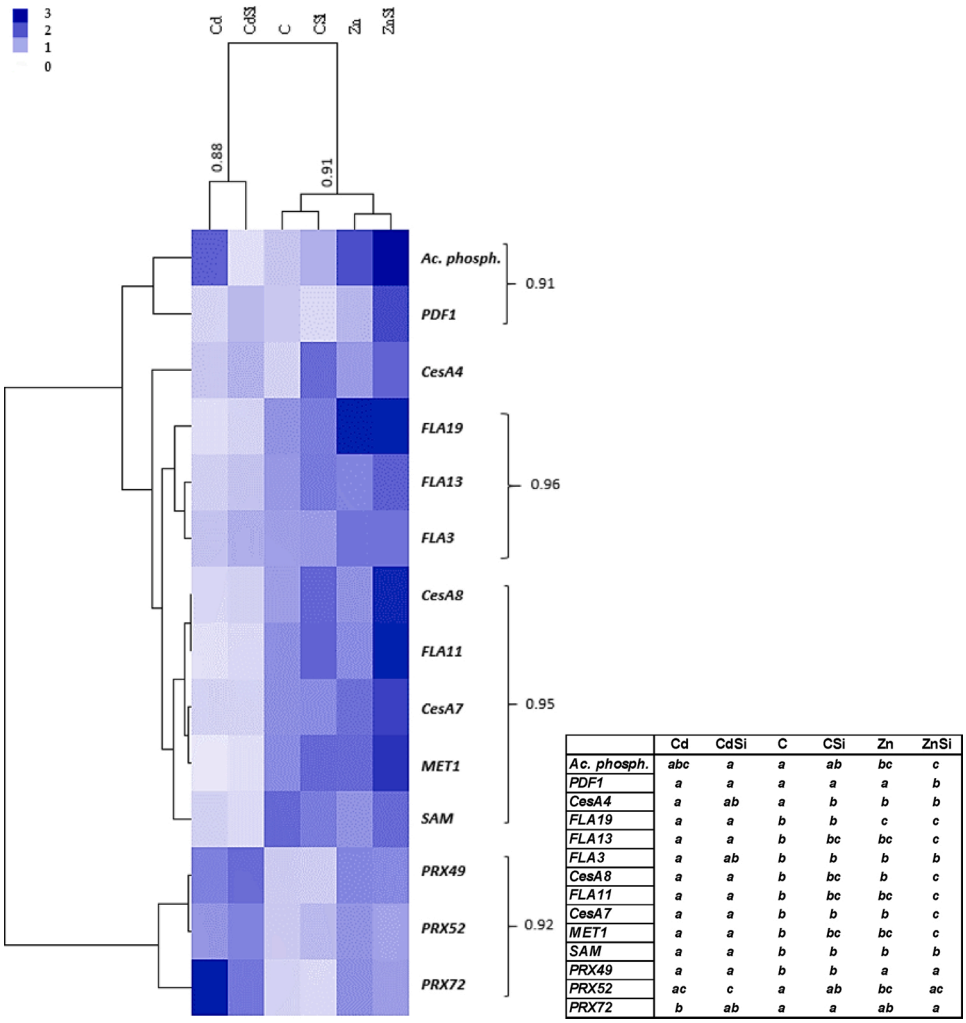

	Cd	CdSi	C	CSi	Zn	ZnSi
Ac. phosph.	abc	a	a	ab	bc	c
PDF1	a	a	a	a	a	b
CesA4	a	ab	a	b	b	b
FLA19	a	a	b	b	c	c
FLA13	a	a	b	bc	bc	c
FLA3	a	ab	b	b	b	b
CesA8	a	a	b	bc	b	c
FLA11	a	a	b	bc	bc	c
CesA7	a	a	b	b	b	c
MET1	a	a	b	bc	bc	c
SAM	a	a	b	b	b	b
PRX49	a	a	b	b	a	a
PRX52	ac	c	a	ab	bc	ac
PRX72	b	ab	a	a	ab	a

Fig. 1. Heatmap hierarchical clustering showing the expression of genes assessed by RT-qPCR in hypocotyls of hemp plants. Plants were exposed for one week to Cd (20 μM) or Zn (100 μM) in the presence or absence of Si (2 mM) (C: control plants not exposed to heavy metals). Values represent Normalized Relative Quantities (NRQs). For each group, the Pearson coefficient is provided. The table represents statistical analyses of the heatmap hierarchical clustering. The different letters indicate that the values are significantly different from each other ($P < 0.05$; Tukey's HSD all-pairwise comparisons).

which catalyses the multi-step methylation reactions of hydroxylated monomeric lignin precursor.

Among proteins up-regulated by Zn exposure (Table 4; Fig. 2), 4 are involved in carbohydrate metabolism, one in callose remodelling (BG), one in CW expansion (monocopper oxidase-like protein SKU5), one in cellulose biosynthesis (SuSy), one in xylan biosynthesis (UDP-glucuronic acid decarboxylase 6-like, UXS), on in SCW synthesis (fasciclin-like arabinogalactan protein 12, FLA12), 2 in lignin biosynthesis (cinnamyl alcohol dehydrogenase 1-like, CAD1; and CYP73A100), one in pectin acetylation (pectin acetylesterase 3-like isoform X2, PAE), one in proline biosynthesis (P5CS), 2 in nitrate and sulphur assimilation (NiR, SIR), one in pyrimidine metabolism, 4 in protein synthesis and 1 in protein folding, 5 in proteolysis, 5 are involved in transport, 3 in ionic homeostasis, one in cell division, 7 in signal transduction and metabolism regulation, and 7 assume key functions in cell rescue. Zn exposure also reduced the abundances of a protein involved in photosynthesis (RuBisCO small subunit), a protein controlling in SCW synthesis (FLA12), a protein controlling the accumulation of crystalline cellulose (glycerophosphodiester phosphodiesterase GDPDL3-like), 2 involved in lignin biosynthesis (LAC4 and CYP736A12), one is involved in amino acid synthesis (aspartate aminotransferase, AAT), one regulating transcription, 16 involved in protein synthesis and folding, one managing in proteolysis, 5 controlling transport, 2 in ionic homeostasis, one in cell organization (actin), 5 playing role in signal transduction and metabolism regulation and 2 involved in cell rescue (catalase, CAT; probable aldo-keto reductase, AKR). The most important category of proteins down-regulated by Zn toxicity were involved in protein processing. It has to be noticed that only a minor proportion of proteins (40) were affected by both Cd and Zn, suggesting that the two heavy metals have a quite different impact on protein regulation in *C. sativa*, despite the fact that they share numerous chemical properties (Jaskulak et al., 2020). When a same protein was affected by both heavy metals, Cd and Zn had similar impacts in terms of up- or down-regulation and no opposite effect was recorded. This was especially the case for LAC4 whose abundance was reduced by both heavy metals, and for glucan endo-1, 3-β-glucosidase (BG) involved in callose degradation which was increased by Cd and by Zn.

The number of proteins affected by Si exposure was by far lower than the number of proteins affected by heavy metals (Table 4 and Fig. 2). Exposure of hemp plants to Si in the absence of heavy metal stress up-regulated proteins involved in photosynthesis (1), amino acid metabolism (MS1), protein synthesis (3), transport (2) and cell rescue (especially MDHAR involved in Asada-Halliwell cycle). Si significantly decreased the accumulation of some proteins involved in photosynthesis (1), SCW formation (FLA12), protein synthesis (4), cell organization (1), signal transduction and metabolism regulation (3) and cell rescue (2). Si had contrasting impact on proteins involved in lignin biosynthesis since it increased the abundance of caffeic acid 3-O-methyltransferase (COMT), while it decreased the abundance of a laccase (LAC4).

Si had a specific impact on some proteins observed in CdSi treatment comparatively to plants exposed to Cd in the absence of Si: 55 % of those proteins (10 among 18) were specifically regulated by this treatment and remained unaffected by Cd or Si applied alone. This was the case for β-D-xylosidase and dehydrorahmnose reductase. Additional Si to Cd-

Table 4
List of proteins with significant quantitative changes of hemp stems in response to Cd, Zn and Si. Seedlings were exposed for one week either to Cd 20 µM, Zn 100 µM or Si 2 mM and proteins were extracted from hypocotyls. MFC: Max Fold Change. Proteins which abundance increased were indicated in green while those which abundance decreased are indicated in brown.

Accession	Soluble protein name	C-Cd		C-Zn		C-CSi		Cd-CdSi		Zn-ZnSi		
		Anova	MFC	Anova	MFC	Anova	MFC	Anova	MFC	Anova	MFC	
Energy												
Photosynthesis/CO2 assimilation												
XP_030478704.1; XP_030510713.1	ribulose bisphosphate carboxylase small chain clone 512-like	↘ 8.44E-03	4.1	↘ 4.62E-02	2.2							rbcS
XP_030501759.1; XP_030499118.1	ribulose bisphosphate carboxylase small chain_ chloroplastic-like							↘ 1.32E-02	2.3			rbcS
XP_030508755.1	dihydrolipoyl dehydrogenase_ mitochondrial-like					↘ 2.39E-02	2.0					
Carbohydrate metabolism, glycolysis and gluconeogenesis												
KAA8710862.1;KPW80790.1	phosphoenolpyruvate carboxylase [Pseudomonas cannabina]	↘ 6.32E-03	2.6									PEPC
XP_030484584.1	phosphoenolpyruvate carboxylase_ housekeeping isozyme-like			↗ 1.45E-03	2.0							PEPC
XP_030496786.1	phosphoenolpyruvate carboxykinase (ATP)-like			↗ 1.11E-03	3.9							PEPCK
XP_030506683.1; XP_030506682.1	pyruvate kinase_ cytosolic isozyme									↘ 2.70E-03	1.6	
XP_030508612.1; XP_030502051.1; XP_030502053.1; XP_030502054.1; XP_030502055.1	galactokinase-like			↗ 1.22E-02	3.1							GALK
XP_030484068.1	probable alpha-mannosidase At5g13980							↘ 7.53E-03	2.7			
XP_030500791.1; XP_030500475.1	plastidial pyruvate kinase 2	↘ 3.35E-03	4.7									PKP2
XP_030484115.1; XP_030484116.1	4-alpha-glucanotransferase DPE2			↗ 5.44E-03	2.4							
XP_030501231.1; XP_030484128.1	glucose-6-phosphate isomerase_ cytosolic					↗ 5.51E-03	2.6					G6PI
Tricarboxylic-acid pathway												
XP_030482299.1	dihydrolipoyllysine-residue acetyltransferase component 4 of pyruvate dehydrogenase complex_ chloroplastic	↘ 4.83E-02	2.0									PDH
XP_030496961.1	aconitate hydratase 1	↗ 3.20E-02	2.2									AH1
XP_030488149.1	NADP-dependent malic enzyme	↗ 2.61E-02	2.0									MDH
Fermentation												
XP_030479792.1	pyruvate decarboxylase 2	↘ 4.84E-03	2.1									PDC2
γ-aminobutyrate (GABA) shunt												
XP_030506646.1	glutamate decarboxylase 4-like	↘ 6.19E-03	3.0									GluDC4
XP_030488867.1; XP_030488649.1	LOW QUALITY PROTEIN: succinate-semialdehyde dehydrogenase_ mitochondrial-like							↗ 2.53E-03	2.2			SSADH
Cell wall related												
XP_030500584.1	monocopper oxidase-like protein SKU5			↗ 1.96E-03	4.4							SKU5
XP_030491523.1; XP_030488795.1; XP_030488796.1; XP_030491522.1	UDP-glucuronic acid decarboxylase 6-like			↗ 2.31E-03	3.3							UXS
XP_030505523.1	fasciclin-like arabinogalactan protein 12			↘ 1.40E-02	2.0	↘ 8.51E-03	2.3					FLA12
XP_030506444.1; XP_030503116.1	fasciclin-like arabinogalactan protein 12			↗ 2.31E-03	3.6							FLA12
XP_030478954.1	glycerophosphodiester phosphodiesterase GDPDL3-like			↘ 3.18E-02	6.0							GDPDL3
XP_030489949,1; XP_030489948,1; XP_030487755,1	caffeic acid 3-O-methyltransferase-like isoform X2	↘ 2.98E-03	3.0									COMT

(*continued on next page*)

Table 4 (*continued*)

XP_030501009.1	caffeic acid 3-O-methyltransferase					↗	1.65E-02	2.2				COMT
XP_030486346.1; XP_030486319.1	cinnamyl alcohol dehydrogenase 1-like			↗	3.60E-02	2.5						CAD
XP_030508841,1; XP_030507959,1	glucan endo-1_3-beta-glucosidase_ basic vacuolar isoform-like	↗	1.28E-03	3.7						↘	4.06E-03	1.5	BG
XP_030508841.1; XP_030507959.1	glucan endo-1_3-beta-glucosidase_ basic vacuolar isoform-like	↗	9.35E-05	5.6	↗	3.91E-03	2.1						BG
XP_030509516.1	putative beta-D-xylosidase							↗	7.60E-03	2.0			BXL
XP_030485245.1	protein TPLATE				↗	4.52E-02	2.1						TPLATE
XP_030488625.1; XP_030488624.1	sucrose synthase-like	↘	2.82E-04	2.3									SuSy
XP_030507721.1	sucrose synthase 7-like				↗	5.92E-05	2.9						SuSy 7
XP_030510687.1	cellulose synthase A catalytic subunit 7 [UDP-forming]	↘	4.66E-02	6.4						↗	3.68E-03	6.3	CesA 7
XP_030494583.1; XP_030480065.1	cellulose synthase A catalytic subunit 8 [UDP-forming]-like	↘	2.88E-03	2.2									CesA 8
XP_030492130.1	methylenetetrahydrofolate reductase 2-like	↘	2.16E-02	2.0									MTHFR
XP_030480227.1	laccase-4-like	↘	5.15E-05	8.1	↘	5.52E-06	6.7	↘	6.79E-04	4.0			LAC4
XP_030496050.1	cytochrome P450 71B34-like	↘	4.19E-05	2.3									CYP71
XP_030506964.1	cytochrome P450 CYP736A12-like	↘	5.17E-03	2.3	↘	6.25E-04	4.3						CYP73
XP_030493605.1	cytochrome P450 CYP73A100-like	↗	4.84E-03	3.7	↗	1.10E-04	2.4						CYP73
XP_030499477.1; XP_030499405.1	pectin acetylesterase 3-like isoform X2				↗	6.68E-04	2.8						PAE
XP_030507468.1	UDP-glucuronate 4-epimerase 6	↘	2.49E-04	3.1									GAE6
XP_030500851.1	bifunctional dTDP-4-dehydrorhamnose 3_5-epimerase/dTDP-4-dehydrorhamnose reductase							↘	3.50E-03	2.2			
METABOLISM													
Amino acids, nitrogen, sulphur and glutathione metabolism													
XP_030488276.1	LOW QUALITY PROTEIN: delta-1-pyrroline-5-carboxylate synthase-like	↗	3.58E-02	2.2	↗	5.12E-04	3.1						P5CS
XP_030486258.1	ferredoxin--nitrite reductase_ chloroplastic-like				↗	3.21E-02	2.6						NiR
XP_030495540.1	S-adenosylmethionine synthase 3	↘	2.65E-04	2.7									SAMs
XP_030503589.1	5-methyltetrahydropteroyltriglutamate--homocysteine methyltransferase 2							↗	1.48E-02	2.8			MS
XP_030483244.1	aspartate aminotransferase P2_ mitochondrial	↘	1.75E-02	2.3	↘	8.03E-04	3.5						AAT
XP_030507269.1; XP_030507270.1; XP_030501899.1; XP_030501900.1	glutamate dehydrogenase 1	↗	3.99E-04	3.6									GluDH
XP_030503475.1	sulfite reductase [ferredoxin]_ chloroplastic	↗	3.36E-05	3.2	↗	1.98E-02	2.2						SIR
Purine, pyrimidine, ribonucleotide and deoxyribonucleotide metabolism													
XP_030481118.1; XP_030479601.1	uracil phosphoribosyltransferase-like				↗	4.38E-02	3.2						UPRT
Protein synthesis, processing, modification													
Transcription													
XP_030505854.1	protein argonaute 4-like				↘	1.00E-02	2.2						
Protein synthesis (ribosomal proteins, translation, tranlational control, amino-acyl tRNA synthetases)													
XP_030500635.1; XP_030489438.1	60S ribosomal protein L15-2				↘	2.38E-02	2.8						L15
XP_030480012.1; XP_030480011.1	60S acidic ribosomal protein P2-2-like	↘	2.00E-02	4.2	↘	3.15E-02	2.5						P2
XP_030503144.1; XP_030488761.1	60S ribosomal protein L10-like				↗	5.46E-03	2.3						L10
XP_030483002.1	60S ribosomal protein L10a				↘	2.55E-02	2.2	↘	4.03E-03	3.0			L10

(*continued on next page*)

Table 4 (*continued*)

XP_030507532.1; XP_030499844.1	60S ribosomal protein L13a-4			↘	6.34E-04	2.2						L13
XP_030491361.1; XP_030489954.1	60S ribosomal protein L14-2-like						↘	3.93E-02	4.0			L14
XP_030480081.1; XP_030494264.1; XP_030501207.1	60S ribosomal protein L18a-2-like isoform X1	↘	4.52E-02	26.8	↘ 9.77E-03	19 2.6						L18
XP_030506326.1; XP_030488101.1; XP_030488102.1; XP_030495139.1	60S ribosomal protein L23a						↘	4.72E-02	23.0			L23
XP_030484025.1; XP_030488290.1; XP_030489190.1	60S ribosomal protein L31	↘	1.54E-02	2.4	↘ 7.49E-07	14.1				↘ 3.55E-02	3.7	L31
XP_030477674.1	60S acidic ribosomal protein P3				↘ 1.70E-04	2.6						P3
XP_030480009.1	60S acidic ribosomal protein P2A-like				↘ 3.70E-02	2.2						P2
XP_030510107.1; XP_030494538.1; XP_030507235.1; XP_030510106.1	40S ribosomal protein S7-like				↗ 8.14E-03	2.2	↗	1.67E-02	2.5			S7
XP_030504232.1	40S ribosomal protein S4-3									↗ 2.40E-02	2.2	S4
XP_030480754.1; XP_030477635.1	40S ribosomal protein S11-like				↘ 4.00E-04	6.1				↘ 9.32E-03	2.8	S11
XP_030488788.1	40S ribosomal protein S3-3				↘ 4.50E-05	2.4						S3
XP_030488957.1	leucine--tRNA ligase_ cytoplasmic	↘	3.75E-02	2.1	↘ 6.81E-03	2.4	↘	2.52E-02	2.1			
XP_030504382.1	elongation factor 1-beta 2	↘	9.98E-05	2.0	↘ 1.17E-03	2.2						EF1
XP_030503776.1; XP_030503775.1	elongation factor 1-alpha						↗	5.62E-03	2.6			EF1
XP_030507726.1	aspartate--tRNA ligase 2_ cytoplasmic	↗	2.07E-02	2.3								
XP_030484605.1	ketol-acid reductoisomerase_ chloroplastic	↗	5.81E-03	2.2								
XP_030481816.1	eukaryotic translation initiation factor 5A-2	↘	1.13E-02	40.9	↘ 5.77E-03	12 3.3						EIF5A2
XP_030491241.1; XP_030490754.1	eukaryotic translation initiation factor 3 subunit K-like				↘ 1.70E-05	5.2						
XP_030486602.1	probable N-acetyl-gamma-glutamyl-phosphate reductase_ chloroplastic				↗ 7.32E-04	3.3						
XP_030499227.1	signal recognition particle receptor subunit beta	↗	1.65E-02	3.4	↗ 5.41E-04	7.9	↗	4.23E-03	7.4			SRPRB
Protein folding and stabilization												
XP_030478962.1	heat shock 70 kDa protein-like				↘ 4.41E-05	3.6						
XP_030498755.1	chaperonin CPN60-2_ mitochondrial-like				↘ 1.06E-02	2.1						CPN60
XP_030490603.1	chaperonin CPN60-like 2_ mitochondrial				↗ 1.17E-02	2.4						CPN60
XP_030488166.1	BAG family molecular chaperone regulator 7	↘	8.64E-04	2.2								BAG7
Proteases												
XP_030484572.1; XP_030493812.1	proteasome subunit alpha type-1-A-like				↗ 1.38E-03	2.3						
XP_030501354.1; XP_030497408.1; XP_030486007.1; XP_030491754.1; XP_030493197.1; XP_030493346.1	ubiquitin-40S ribosomal protein S27a	↗	1.28E-02	2.1	↗ 5.88E-03	2.3						UBQ
XP_030491503.1	ubiquitin carboxyl-terminal hydrolase 6-like				↘ 5.93E-04	5.0						UCH6
XP_030508051.1; XP_030508052.1	cullin-1	↗	2.78E-03	2.9	↗ 6.76E-03	2.2						CUL1
XP_030490048.1; XP_030490049.1	F-box/kelch-repeat protein SKIP4										↘ 4.30E-03	2.8 SKIP4
XP_030496958.1	subtilisin-like protease SBT1.7	↗	5.23E-03	3.4	↗ 3.85E-03	4.4						SBT1
XP_030509608.1; XP_030509609.1	subtilisin-like protease SBT5.3 isoform X1									↗ 1.95E-03	3.4	SBT5
XP_030485032.1	probable cysteine protease RD19B				↗ 2.84E-05	2.8						
Transport facilitation, transport mechanism, membrane modification												
XP_030507209.1	importin subunit alpha-1-like				↘ 1.46E-02	2.1						
XP_030505754.1	ras-related protein RABA2a				↗ 4.21E-02	2.4						RABA2
XP_030488383.1	pleiotropic drug resistance protein 1-like	↗	2.37E-02	2.4	↗ 2.73E-02	2.6						PDR1
XP_030489689.1; XP_030489690.1; XP_030489691.1;	protein FATTY ACID EXPORT 3_ chloroplastic isoform X1	↗	1.17E-02	2.1								FAX1

(*continued on next page*)

Table 4 (*continued*)

XP_030489692.1; XP_030489693.1										
XP_030491831.1	pyrophosphate-energized vacuolar membrane proton pump-like	↘	6.08E-03	2.5	↘	4.87E-04	2.9			
XP_030495608.1	ras-related protein RABC2a-like				↘	1.31E-02	2.2			RABC2
XP_030505782.1	guanosine nucleotide diphosphate dissociation inhibitor At5g09550				↘	2.38E-02	2.2			
XP_030502238.1	dynamin-related protein 1E-like							↗	2.41E-02	2.0			DRP1
XP_030480160.1	gamma-soluble NSF attachment protein				↘	1.83E-02	4.3			
XP_030480614.1	vesicle-associated membrane protein 711	↗	1.21E-03	3.0						VAMP711
XP_030507156.1; XP_030507155.1	vesicle-associated protein 2-1-like isoform X2							↗	2.80E-02	2.1			VAMP2
XP_030488587.1; XP_030488355.1	LOW QUALITY PROTEIN: coatomer subunit beta'-1-like				↗	2.80E-02	2.3			
XP_030479858.1	clathrin light chain 2-like				↗	2.73E-02	2.0			CLC2
XP_030496965.1; XP_030496964.1	putative clathrin assembly protein At2g01600 isoform X2				↗	9.82E-07	2.7			
XP_030499077.1	AP-1 complex subunit gamma-2-like										↗	1.08E-02	2.5	
XP_030477745.1	transmembrane 9 superfamily member 11	↘	3.85E-02	4.6										TMN11
Ionic homeostasis														
XP_030489388.1	copper transporter 5.1-like				↗	7.07E-04	2.9							COPT
XP_030489759.1	proton pump-interactor 1	↗	9.59E-04	2.1	↗	1.75E-05	3.1							PPI1
XP_030483484,1	plasma membrane ATPase 4	↗	3.39E-03	2.2										
XP_030477717.1	plasma membrane ATPase 4-like				↘	2.50E-04	3.6							
XP_030495866.1	ABC transporter C family member 3-like	↗	9.93E-03	4.2										
XP_030493045.1; XP_030493046.1	ABC transporter E family member 2				↘	2.09E-02	10.3				↘	6.58E-03	8.0	
XP_030491043.1	oligopeptide transporter 3	↗	5.26E-05	3.6	↗	3.82E-05	6.6							OPT3
Cell division, cell organisation														
Cell division														
XP_030501768.1	protein FIZZY-RELATED 2-like				↗	3.66E-03	3.0							
Cellular organization (organization of cytoskeleton)														
XP_030482459.1	tubulin alpha-1 chain	↘	4.15E-02	2.6										
XP_030481404.1	tubulin beta-1 chain	↘	9.78E-04	2.6										
XP_030496340.1	tubulin alpha-3 chain	↘	8.25E-03	2.1										
XP_030499509.1; XP_030499508.1	actin-7	↘	3.16E-02	2.2	↘	1.94E-04	5.7	↘	2.22E-02	2.3	↘	1.11E-02	2.6	
XP_030495750.1	LOW QUALITY PROTEIN: villin-3-like	↗	1.39E-02	3.0							↘	2.00E-02	2.6	VLN3
Signal transduction and metabolism regulation														
XP_030496860.1; XP_030496861.1	14-3-3 protein 1 isoform X1				↘	5.93E-03	2.3							14-3-3
XP_030484623.1; XP_030484622.1	14-3-3-like protein B isoform X2	↗	4.00E-02	2.9	↗	2.93E-02	2.6							14-3-3
XP_030503150.1	calreticulin							↘	4.66E-02	2.6				CRT
XP_030485891.1	phosphoinositide phosphatase SAC7-like	↘	2.77E-02	4.1										SAC7
XP_030504426.1	G-type lectin S-receptor-like serine/threonine-protein kinase RLK1				↗	2.84E-02	5.0							LecRLK1
XP_030498105.1	probable serine/threonine-protein kinase PBL21				↗	2.09E-05	4.7				↗	3.36E-02	2.7	
XP_030496318.1	leucine-rich repeat receptor-like serine/threonine-protein kinase BAM1				↗	1.82E-03	9.9							BAM1
XP_030486886.1; XP_030487730.1	annexin-like protein RJ4	↗	1.32E-02	3.8	↗	1.92E-02	2.6							
XP_030497088.1	spermidine synthase 1	↘	1.91E-02	3.3	↘	1.78E-02	3.5							SPDS
XP_030500392.1	RGG repeats nuclear RNA binding protein A	↘	1.95E-02	10.8	↘	4.58E-02	5.2	↘	1.63E-02	7.4				RGGA
XP_030504790.1	protein AUXIN RESPONSE 4		2.65E-02	8.3										
XP_030486567.1	allene oxide synthase 3-like				↗	1.13E-03	2.3							AOS3

(*continued on next page*)

Table 4 (*continued*)

XP_030480062.1	WD repeat-containing protein 44	↘	1.71E-03	3.1	↘	3.05E-02	2.0	↘	3.60E-03	2.6		WD-44
XP_030483052.1; XP_030502571.1	protein TRANSPARENT TESTA 9-like	↗	2.56E-02	2.0								TT9
XP_030503439.1; XP_030503440.1	mitochondrial Rho GTPase 1-like	↘	6.02E-03	2.6	↘	4.98E-04	5.1					MIRO1
XP_030507175.1	GTP-binding protein SAR1A-like	↗	1.22E-02	3.2	↗	2.40E-02	2.1					SAR1A
XP_030507283.1	apyrase 2-like	↘	1.74E-04	5.1								APY2
Cell rescue, defense												
XP_030501451,1	pathogenesis-related protein R major form-like	↗	4.57E-03	4.5								PRR
XP_030487534.1	pathogenesis-related protein 1-like	↗	3.63E-05	26.5	↗	1.25E-04	8.4					PR1
XP_030502231,1	thaumatin-like protein 1	↗	6.83E-03	2.6								TLP
XP_030485657,1	endochitinase 2	↗	1.04E-03	4.8	↗	3.35E-02	2.1					ECH2
XP_030485657,1	endochitinase 2	↗	3.80E-03	11.9								ECH2
XP_030510068.1	class V chitinase-like	↘	6.86E-04	2.2								CH5
XP_030506215.1; XP_030503115.1	barwin-like	↗	3.24E-02	7.1								
XP_030507759.1; XP_030507760.1	probable aldo-keto reductase 2							↗	3.96E-02	2.4		AKR
XP_030507759.1; XP_030507760.1; XP_030507758.1	probable aldo-keto reductase 2	↗	1.99E-03	3.6	↗	5.57E-05	5.5	↗	2.49E-02	2.7		AKR
XP_030508067.1	universal stress protein PHOS32							↘	6.27E-03	2.1		
XP_030508067.1	universal stress protein PHOS32	↗	1.43E-04	2.7								
XP_030486303.1	cyclase-like protein 2	↗	2.42E-02	3.5	↗	2.26E-02	4.3					CYCL2
XP_030498132.1	catalase-2				↘	3.78E-02	2.9					CAT
XP_030493815.1	catalase isozyme 2-like	↗	4.49E-02	2.2								CAT
XP_030499793.1	peroxidase 72				↗	2.62E-02	2.7					PRX
XP_030479401,1	peroxidase 15-like	↗	4.02E-02	2.5								PRX
XP_030485526.1	peroxidase 4-like	↗	5.44E-05	2.2								PRX
XP_030501341.1	monodehydroascorbate reductase_ chloroplastic/mitochondrial				↗	1.17E-02	4.9	↗	3.80E-02	3.2		MDHAR
XP_030504138.1	CBS domain-containing protein CBSX3_ mitochondrial	↗	6.63E-04	2.2								CBSX3
XP_030507868.1	aldehyde dehydrogenase 22A1				↘	1.39E-02	10.5	↘	1.87E-02	9.3		ALDH
XP_030481542.1	formate dehydrogenase_ mitochondrial	↗	2.64E-05	3.6								FDH
XP_030494341.1; XP_030494342.1; XP_030495485.1	L-galactono-1_4-lactone dehydrogenase_ mitochondrial-like				↗	1.04E-02	17.2					GLDH
XP_030498417.1	phosphoprotein ECPP44-like	↗	1.69E-02	3.1								
Others												
XP_030508375.1	probable monoterpene synthase MTS1_ chloroplastic										↘ 1.58E-02	1.9 MTS1
XP_030510929.1	farnesyl pyrophosphate synthase-like				↘	3.58E-02	2.4					FPPS
XP_030508570.1	gamma conglutin 1-like	↗	9.39E-03	2.5								TM9SF9
XP_030478866.1	transmembrane 9 superfamily member 9-like	↘	1.51E-02	2.0								
XP_030480855.1; XP_030480856.1	prosaposin-like				↗	1.50E-04	3.5					
XP_030507618.1	3-ketoacyl-CoA thiolase 2_ peroxisomal				↗	4.15E-03	2.2					KAT2
XP_030485010.1; XP_030485011.1	DExH-box ATP-dependent RNA helicase DExH17 isoform X1	↘	4.28E-02	3.7	↘	5.14E-07	24.3	↘	4.45E-02	2.8		
XP_030489288.1	serine carboxypeptidase-like										↗ 2.10E-02	2.2 SCPL
XP_030507087.1	probable methyltransferase PMT3	↘	1.13E-03	11.4	↘	4.96E-03	3.4					PMT3
XP_030490122.1	probable methyltransferase PMT13				↗	6.74E-03	6.0				↗ 3.87E-02	2.3 PMT13
XP_030501398.1	probable methyltransferase PMT14	↘	3.53E-03	2.6								PMT14
XP_030499403.1	stemmadenine O-acetyltransferase-like	↗	1.10E-03	2.5	↗	1.60E-06	5.7					

(*continued on next page*)

Table 4 (*continued*)

XP_030484735.1; XP_030484734.1	peroxisomal and mitochondrial division factor 1	↗	3.60E-03	4.6						PMD 1
XP_030508261.1	gamma conglutin 1-like	↗	3.83E-04	8.4	↗	2.30E-03	3.5			
No assigned function										
XP_030492112.1	uncharacterized protein LOC115708075	↗	4.91E-02	2.2						
XP_030505388.1	uncharacterized protein LOC115720376				↘	3.12E-02	2.6			
XP_030485083.1	uncharacterized protein At5g39570				↗	1.87E-02	2.0			
XP_030488475.1; XP_030488483.1	protein unc-13 homolog isoform X1	↘	6.29E-03	5.9	↘	4.95E-02	2.7			
XP_030503417.1	probable inactive receptor kinase At5g58300	↘	1.33E-02	2.0						
XP_030487712.1	uncharacterized protein LOC115704652	↗	6.44E-05	28.6	↗	2.30E-03	4.8			
XP_030479238.1; XP_030497626.1; XP_030502429.1; XP_030502664.1	uncharacterized protein LOC115696478	↗	3.62E-03	5.9	↗	1.02E-02	2.4	↗ 2.30E-02	2.3	↘ 2.40E-02 3.2
XP_030485083.1	uncharacterized protein At5g39570				↘	3.27E-03	2.1			
XP_030508867.1	LOW QUALITY PROTEIN: uncharacterized protein LOC115723511_ partial				↗	3.78E-02	4.2			
XP_030481950.1	uncharacterized protein At1g08160-like				↗	1.21E-02	2.5			
ARE72265.1	IDI_ partial									↘ 4.44E-02 2.3

treated plants had no impact on other CW-related proteins previously mentioned to be affected by Cd treatment. Only 6 proteins were significantly regulated in ZnSi-exposed plants comparatively to Zn-treated ones and none of them were specifically regulated by Si in the absence of Zn. Similarly, one glucan endo 1,3-β-glucosidase and cellulose synthase A were respectively down- and up-regulated in response to ZnSi while these proteins were not affected by Si or by Zn applied separately.

3.5. Confocal microscopy and immunohistochemistry

Confocal microscope observation of stem sections (Fig. 3) revealed that Cd-treated plants displayed a lower level of lignin than controls and Zn-treated plants diplayed the highest proportion of lignin comparatively to control (C) or Cd-treated plants.

Confocal microscope observations were also carried out on 3 plants per treatment for immunochemistry. A monoclonal antibody recognizing xylan (LM10) and His-tagged recombinant protein recognizing crystalline cellulose (CBM3a) were used to study the impact of heavy metals on bast fibre development.

Figs. 4 and 5 allowed us to observe the histological modifications induced by heavy metals in the stem, as well as the impact of Si. In all plant sections, secondary growth can be observed by the presence of cambial cells and the typical radial organization of secondary xylem vessels. This radial organization was less marked for plants of Cd treatment without Si supply. Primary and secondary bast fibres were easily distinguishable in the stems of all treatments, except in stems of Cd-treated plants. The diameter of primary and secondary bast fibres was measured for each treatment. In plants of Cd treatment, the differentiation stage of secondary bast fibres was not compatible with an analysis. The diameter decreased in both types of bast fibres when plants were exposed to heavy metals (Cd and Zn, Fig. 6). Interestingly, the diameter increased in Cd-stressed plants when they were simultaneously exposed to Si, but this was not observed for Zn-treated plants. Both diameter and thickness of xylem vessels (Fig. 7) were smaller in plants exposed to Cd or Zn, with a contrasting effect of Si on the diameter of Cd and Zn treatments since it increased in Cd-stressed plants and decreased in plants treated with Zn.

On sections observed at the confocal microscope (Fig. 4), the xylan epitope was detected mainly in xylem cells (x) and in the C of primary bast fibres (pf). In Cd, CdSi and Zn-treated plants a clear signal was also detected in collenchyma cells (c) (Table 5). The walls of primary bast fibres were more strongly labelled by this antibody in Cd-treated plants as compared to control ones. Si decreased the signal intensity in the collenchyma of Zn-treated plants. Using the ImageJ program, we measured the thickness of the signal distribution in bast fibres. The results presented in Table 5 show that in plants exposed to Cd or Zn, the thickness significantly decreased as compared to control plants. The same observation can be made when control plants are treated with Si (Table 5).

Crystalline cellulose was visualized with CBM3a. It was observed in all tissues, especially in collenchyma, xylem cells and in both primary and secondary bast fibres (Fig. 5). In the case of Cd-treated plants, the signal from secondary bast fibres was not detected but we saw an effect of Si in the case of Cd-treated plants: the differentiation stage of secondary bast fibres was sufficient to detect a signal. (Fig. 5). In Cd and Zn-treated plants, primary bast fibres displayed a more intense signal than the one detected in control plants. On the contrary, the signal was less intense in secondary fibres for the same plants (Fig. 5, Table 6). The thickness of the fibres as detected with the CBM3a signal, was influenced by the heavy metal treatment: it decreased in primary bast fibres of Cd-exposed plants and in secondary fibres of Zn-treated plants (Table 6).

4. Discussion

Cd and Zn are well known environmental pollutants which negatively affect plant growth and biomass production. Si has frequently been reported to protect plants from heavy metal toxicity (Adrees et al., 2015; Neumann and zur Nieden, 2001; Wu et al., 2013; Imtiaz et al., 2016). The present work confirms the deleterious impact of Cd and Zn on root and shoot growth in hemp and also highlights that both elements reduced the diameter of primary bast fibres, suggesting that these pollutants may have a negative impact on fibre yield in *C. sativa*. Although exogenous Si tended to improve the behaviour of plants exposed to heavy metals, such a positive impact remained unsignificant which could be partly explained by the high level of intraspecific variability still present in most hemp cultivars (García-Tejero et al., 2019; Mihoc et al., 2012; Jenkins and Orsburn, 2020), but also by the short duration of the simultaneous exposure to Si and heavy metals: it might indeed be argued that one week was not sufficient to detect the significant

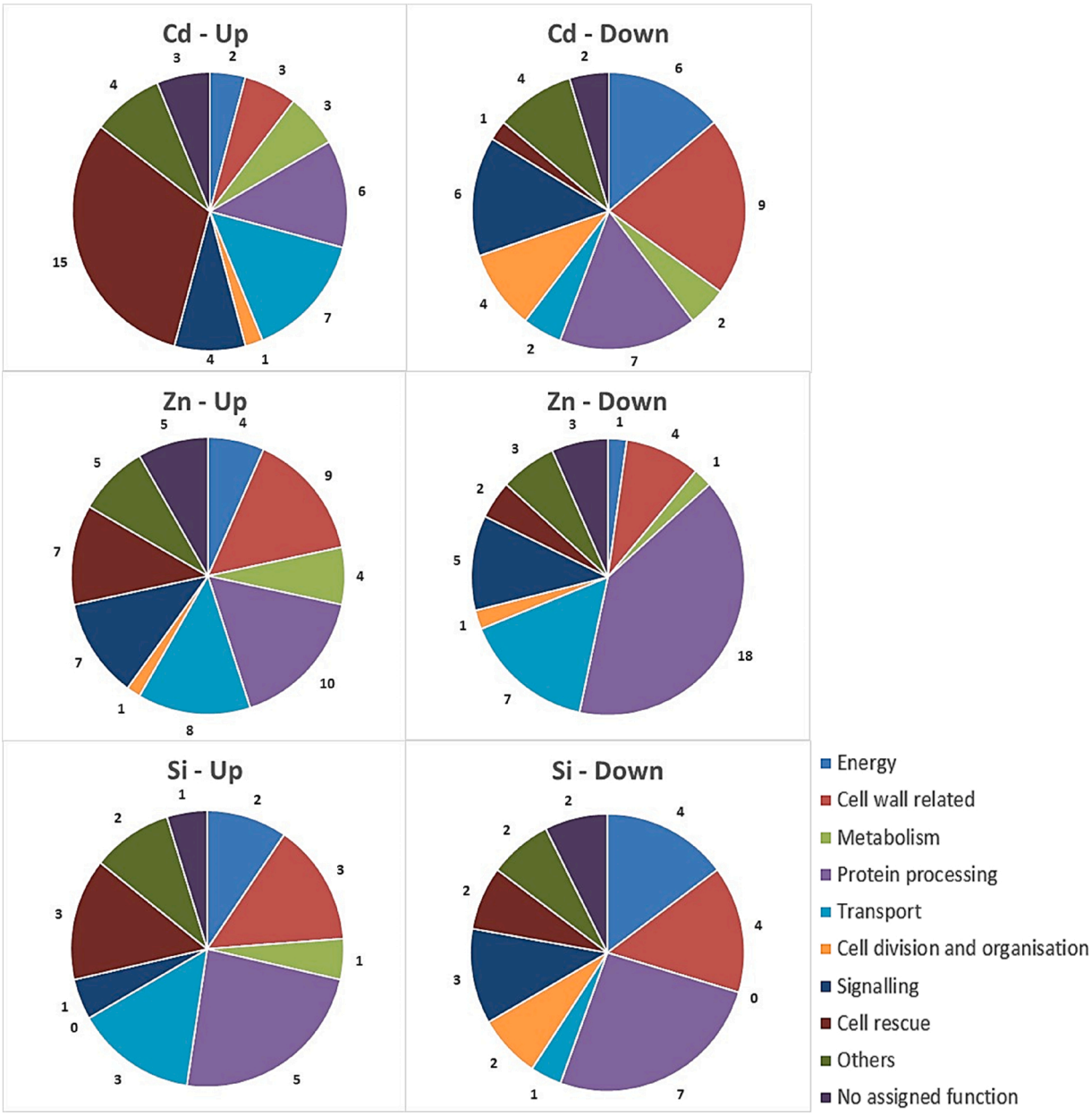

Fig. 2. Functional classification of proteins with significant quantitative changes in abundance in hemp hypocotyls in response to Cd, Zn and Si. Seedlings were exposed for one week either to Cd 20 μM, Zn 100 μM or Si 2 mM and proteins were extracted from hypocotyls. Mixed treatment (CSi, CdSi, ZnSi) are not indicated for the sake of clarity.

advantage conferred by Si to the growth of Cd- and Zn-treated plants, even if it allowed us to detect the impact of Si on some gene expression and specific protein abundances (see below).

A high concentration of Cd was recorded in roots and shoots of *C. sativa* after one week of treatment, reflecting the capacity of hemp to absorb and accumulate this toxic element. The recorded values were higher than those mentioned in the literature (Citterio et al., 2003; Angelova et al., 2004; Meers et al., 2005) which could be due to the fact that the present experiment was conducted in nutrient solution rather than in soils where Cd bioavailability constitutes a limiting factor for Cd absorbtion. Cd and Zn accumulations in stems and leaves of heavy-metal treated plants (expressed relative to the corresponding organ DW basis) were in the same order of magnitude, while Si accumulation in the stem of the Si-treated plants was clearly lower than in roots which are in close contact with the Si-containing nutrient solution, and in leaves which represent evaporative organs where accumulation of passively translocated elements may occur. The low level of Si accumulation in stems, however, does not preclude a significant effect of Si on stem metabolism and mechanical properties. Indeed, Si is not uniformly distributed in plant tissues and accumulates at specific sites (Guerriero et al., 2020). As far as hemp stem is concerned, SIMS nano-analysis revealed the presence of Si in the distal CW of bast fibres (Guerriero et al., 2019).

Heavy metals also accumulate within the CW and this represents an efficient strategy preventing heavy metal accumulation in the cytosol. Vacuolar compartmentation of toxic elements is also considered as a valuable option for improving cell resistance (Sharma et al., 2016) and a positive effect of Cd on ABC transporters and oligopeptides transporters recorded in our study may be regarded as an attempt to limit Cd accumulation in the cytosol. Additional Si had a dual impact on these processes since it reduced the abundance of ABC transporters, but obviously increased the abundance of a protein involved in vesicular trafficking.

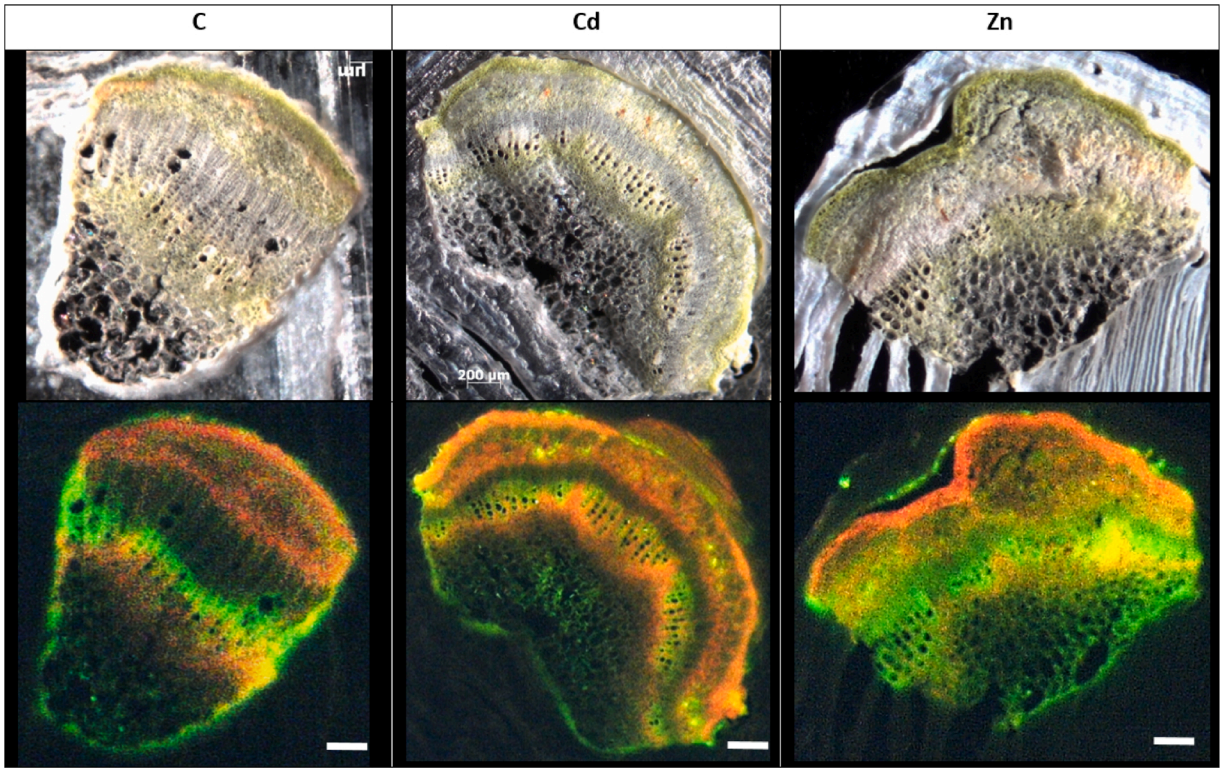

Fig. 3. Confocal microscope observation of hemp stem sections (60 µm) (Axioscope 2 MOT, 405 nm). Plants were exposed for one week to Cd (20 µM) or Zn (100 µM) (C: control plants not exposed to heavy metals). Fluorescence highlights lignified areas (yellow), areas containing chlorophyll (orange-red color), and simple phenols compounds (green). Scale bar: 200 µm.

Neumann and zur Nieden (2001) demonstrated in the Zn-resistant plant *Arabidopsis halleri* that Zn transiently accumulates as silicate in vacuolar vesicles and to a lower extent in the cytosol before being translocated to vacuoles where Zn-silicates are slowly degraded to SiO_2. This clearly suggests that Si distribution is not limited to the apoplasm.

Besides vacuolar sequestration, cell to cell trafficking constitutes a strategy to dilute heavy metals in the symplasm avoiding these ions to reach toxic levels. Callose (β-1,3-glucan) regulates plasmodesmatal permeability since an increase in plasmodesmata-localized callose is associated with a decrease in plasmodesmatal aperture (O'Lexy et al., 2018). In *A. thaliana*, O'Lexy et al. (2018) reported that Cd reduced plasmodesmatal permeability but our data on hemp stem provide a different picture since Cd and Zn increased the abundance of β-1, 3-glucosidase (BG) involved in callose breakdown. In contrast, Si reduced BG abundance in heavy-metal treated plants which may limit Cd and Zn mobility between cells. Silica precipitation may indeed be induced by callose which was shown to play a key role in silification of Si-accumulating species like *Equisetum arvense* and *Oryza sativa* (Guerriero et al., 2018a, 2018b, 2020).

After one week of treatment, heavy metals affected numerous proteins playing important roles in cell metabolism. Heavy metal toxicity is known to disturb photosynthesis and the fact that Cd and Zn decreased RuBisCO subunit was not unexpected. It is interesting to note, however, that in our study heavy metals mainly act on the chloroplastic small subunit confirming that this organelle is particularly sensitive to the deleterious effect of Cd and Zn (Lefèvre et al., 2014; Chandra and Kang, 2016). Cd also affected numerous enzymes involved in TCA cycle which could be related to an increase in the requirement of energy to cope with stress. In contrast, Zn excess did not directly impact TCA cycle but affected carbohydrate metabolism through an increase in DPE2 involved in maltose breakdown to glucose and by affecting the abundance of GALK which contributes to the synthesis of glucose-1-phosphate.

The non-protein amino-acid γ-aminobutyric acid (GABA) is assuming important functions in stress metabolism and signaling in plants and is synthesized via calcium/calmodulin-dependent glutamate decarboxylase activity (GluDC) (Seifikalhor et al., 2019). GluDC was strongly reduced in Cd-treated plants, but this should not be necessarily regarded as a symptom of injury and could be explained by the crucial role of glutamate as a precursor of other important molecules for stressed plants: glutamate is indeed converted to 2-oxoglutarate by glutamate dehydrogenase to fuel the TCA cycle and it is a precursor of proline which is a valuable protecting compound frequently overproduced in various stress conditions and which is suspected to directly chelate heavy metals (Lefèvre et al., 2014; Seifikalhor et al., 2019). The recorded increased abundance of P5CS (catalyzing the rate-limiting step of proline synthesis) in Cd- and in Zn-treated plants, supports the hypothesis that glutamate should remain available for the synthesis of this osmoprotectant. Glutamate is also an important precursor of the endogenous antoxidant glutathione (GSH) which is itself involved in the synthesis of phytochelatins (PC) directly implicated in heavy metal binding to cysteine, the complex being subsequently sequestered in vacuoles. Such a protecting process is especially efficient in response to Cd toxicity which triggers PC overproduction (Lefèvre et al., 2016).

A specific attention was paid to SCW deposition and a global overview of the impact of Cd and Zn on the synthesis of CW precursor is provided in Fig. 8. We studied gene expression and protein abundance in the hypocotyls of 28 days-old plants. At this stage, secondary xylem and secondary bast fibres, together with primary bast fibres, undergo SCW deposition (Behr, 2018). We analysed genes coding for bast fibre early growth stage (*PDF1*), genes involved in the transition from elongation to thickening (acid phosphatase, *AT1G04040*) and genes involved in SCW deposition (*CesA4, CesA7 and CesA8*, class III peroxidases, *MET1* and *SAMS*).

Protodermal factor 1 (*PDF1*) is likely regulating hemp bast fibre early growth (Guerriero et al., 2017a). In 28-days hemp hypocotyls, fibres have completed their elongation and have started SCW deposition. Si

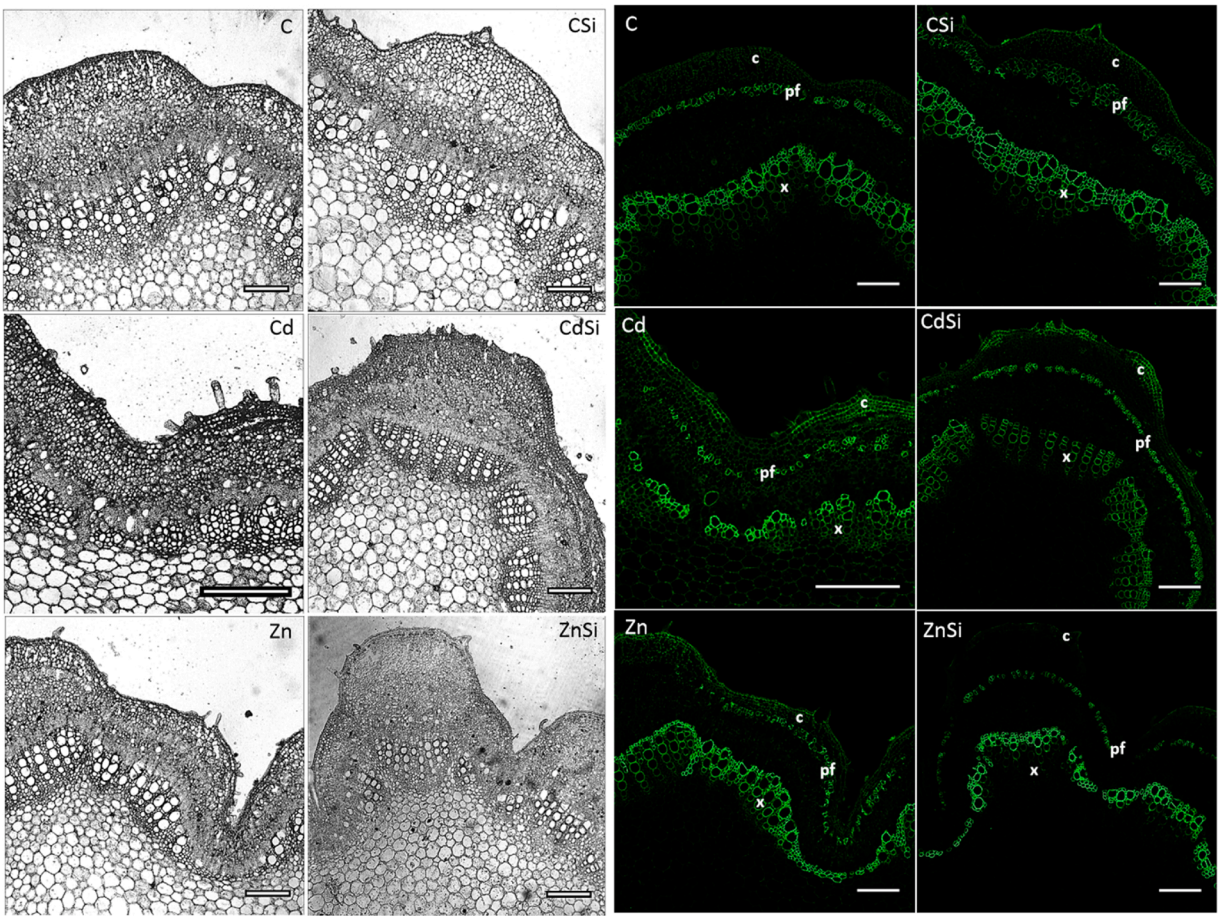

Fig. 4. Confocal microscope observation and immunodetection of the LM10 epitope specific for xylan in stem sections of *Cannabis sativa* (cv. Santhica 27). Plants were exposed for one week to Cd (20 μM) or Zn (100 μM) in the presence or in the absence of Si 2 mM. Control plants (C), Cd (Cd-treated plants), Zn (Zn-treated plants), with or without silicon (Si). Primary bast fibre (pf), secondary bast fibre (sf), xylem (x). Scale bar: 200 μm.

application induced an increased expression level of *PDF1* for plants exposed to Zn and to a lower extent to Cd (not significant) treatments. Similarly, acid phosphatase is controlling CW-related processes in bast fibres during the transition from elongation to thickening (Guerriero et al., 2017a) and appears to be more expressed in Cd- and Zn-stressed plants compared to control ones. These data suggest that the timing of fibre elongation and transition from elongation to thickening may be affected by heavy metals and that Si may have an influence on this process.

Cd and Zn had contrasting effects on genes and proteins involved in SCW deposition. While Cd negatively affected gene expression and protein abundance involved in CW deposition, Zn had an opposite impact although it did not act on the same target. Indeed, plants exposed to Cd showed a lower expression of two genes coding for the cellulose synthases *CesA7* and *CesA8*, while in Zn-stressed plant CesA4 expression level increased. *CesA4*, *CesA7* and *CesA8* are usually associated with SCW biogenesis in both xylan-type and gelatinous-type SCW (Taylor et al., 2003; Gorshkova et al., 2012). They are therefore regulating the deposition of the SCW in both tissues (Behr, 2018). Our sample contained both bast fibres in the cortical part of the stem and xylem tissues in the core. It is therefore difficult to attribute the expression of these genes to xylan-type or gelatinous-type SCW. However, a recent study performed on flax has highlighted that both PCW- and SCW-related CesAs have a higher expression in phloem fibres depositing their G-layer (Mokshina et al., 2017). Our proteomic data corroborated transcriptomic results since Cd clearly decreased the abundance of CESA7 and CESA8 (Fig. 8).

To visualize Cd and Zn effect on cellulose deposition in stems, we performed confocal microscope observations of His-tagged recombinant protein recognizing crystalline cellulose (CBM3a). In Cd and Zn treated plants, primary bast fibres displayed a signal that was more intense than the one detected in control plants, while abundance of CESA7 and CESA8 was shown to increase in Cd treated plants. Secondary bast fibres were not detected under Cd treatment. In Zn- and CdSi-treated plants, the signal was less intense than in control plants. It may therefore be hypothesized that heavy metals could modify bast fibres properties in relation to the decrease in cellulose abundance and to affect cellulose crystallinity detected by the recombinant protein used, although CBM3a is not fully specific to crystalline cellulose since it may also recognize xyloglucan present in PCW (Hernandez-Gomez et al., 2015). A Zn-induced decrease in GDPDL3 controling cellulose crystallisation (Fig. 8) as well as a decrease in the thickness of distribution of the CBM3a signal in primary (and secondary for CdSi-exposed plants) bast fibres of Cd-exposed plants and in secondary fibres of Zn-treated plants support this hypothesis. It could not be excluded, however, that cell wall modification possiby induced by heavy metals can also modify epitope accessibility, thus accounting for reduction of labelling. Cd (but not Zn!) also decreased the abundance of sucrose synthase (SuSy; Fig. 8) isoforms which provide UDP-glucose to cellulose synthase (Granot and Stein, 2019) and this may also contribute to alter cellulose synthesis in Cd-treated plants. The addition of Si to Cd-treated plants did not counteract the impact of Cd on gene expression or protein abundance, which clearly shows that Si may act on specific cues and must not be regarded as a Cd antagonist.

Fasciclin-like arabinogalactan proteins are cell surface proteins linked to CW deposition and stem development in many species, from

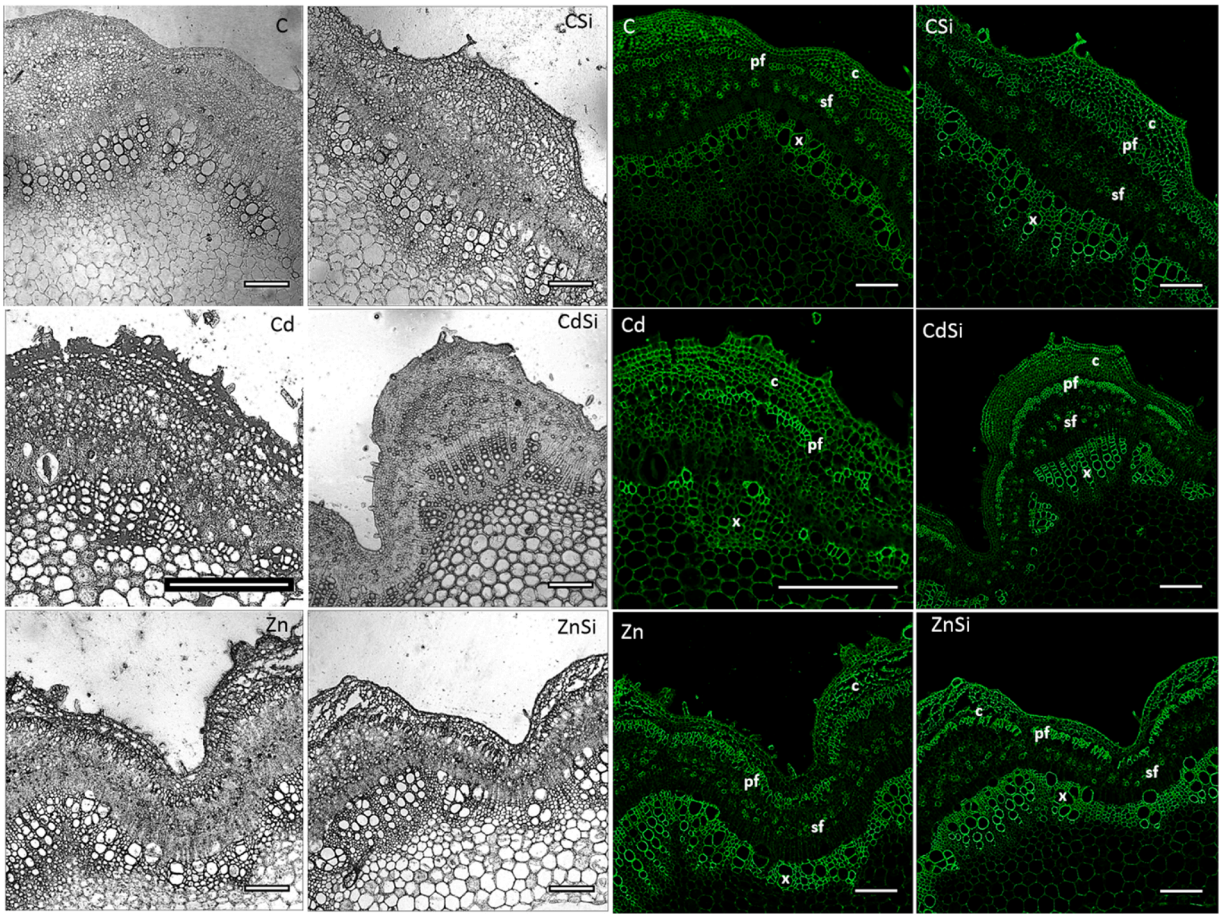

Fig. 5. Confocal microscope observation and immunodetection of the CBM3a epitope specific for crystalline cellulose in stem sections of *Cannabis sativa* (cv. Santhica 27). Plants were exposed for one week to Cd (20 μM) or Zn (100 μM) in the presence or in the absence of Si 2 mM. Control plants (C), Cd (cadmium treated plants), Zn (zinc treated plants), with or without silicon (Si). Primary bast fibre (pf), secondary bast fibre (sf), xylem (x). Scale bar: 200 μm.

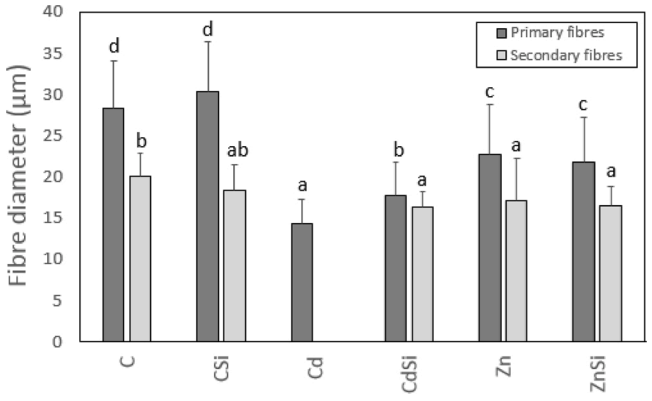

Fig. 6. Diameter of primary (FI) and secondary (FII) bast fibres in stems of *Cannabis sativa* (cv. Santhica 27). Plants were exposed for one week to Cd (20 μM) or Zn (100 μM) in the presence or in the absence of Si 2 mM. FII were not detected in Cd treated plants. The different letters indicate that the values are significantly different from each other ($P < 0.05$; Tukey's HSD all-pairwise comparisons). $n = 15$ (3 plants/treatment, 5 fibres/plant).

herbaceous to woody (Behr, 2018). In hemp, Guerriero et al. (2017b) identified specific *FLAs* likely involved in SCW deposition during the thickening stage (*CsaFLA3-12-13-15-16-18-19*; Guerriero et al., 2017b). In our hemp hypocotyls, the number of transcripts of *FLA3, FLA13*, *FLA11* and *FLA19* was lower for Cd-stressed plants and *FLA19* expression was higher for Zn stressed plants compared to controls, confirming once again a differential impact of the two considered heavy metals. *CsFLA13* and *CsFLA19* are highly expressed at the snap point as well as in older stem region (Guerriero et al., 2017b) and this might indicate a specific role in secondary growth. The concerted action of specific FLAs and chitinases may be involved in the transition from elongation to G-layer formation in hemp via the cleavage of the GlcNAc oligosaccharides part of FLA (Guerriero et al., 2017b): two endochitinase were increased in Cd-treated plants but their involvement in interaction with FLA is not demonstrated at this stage and requires further investigations

The present work demonstrates that Cd reduced the abundance of enzymes regulating lignin biosynthesis (decrease in COMT, CytP450, MTHFR, LAC4, CYP736A12; Fig. 8), while the situation was less clear for Zn which increased CAD1 but decreased LAC4 and CYP736A12. This contrasts with the results obtained in *Medicago sativa* where Cd exposure increased numerous proteins involved in the promotion of lignifiction (Gutsch et al., 2018). Hence, plant response may differ according to the species but also depending on stress duration: Gutsch et al. (2018) applied a long term Cd treatment while we recorded the data after one week only. Lignin is mainly present in shivs while bast fibres contain between 2–7 % lignin only (Guerriero et al., 2017a). Despite being a minor component in bast fibres, lignin is deposited in the S1-layer for mechanical reasons as the hypocotyl ages (Behr et al., 2019) and lignin in hemp bast fibres is rich in S-units as the hypocotyl ages, because of the high abundances of enzymes regulating monolignol methylation (Behr et al., 2018). It is well established that apoplastic H_2O_2 is important for lignification processes and it functions as a signaling molecule triggering enzymatic activities like those of CW-localized peroxidases (Cosio and Dunand, 2008; Gutsch et al., 2019a). A role of peroxidases in fibre

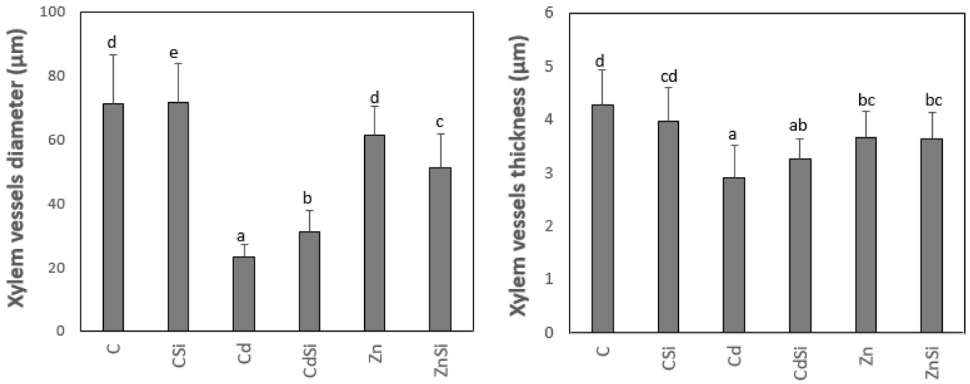

Fig. 7. Diameter and thickness of the xylem vessels cell walls in stems of *Cannabis sativa* (cv. Santhica 27). Plants were exposed for one week to Cd (20 µM) or Zn (100 µM) in the presence or in the absence of Si 2 mM. The different letters indicate that the values are significantly different from each other ($P < 0.05$; Tukey's HSD all-pairwise comparisons). n = 30 (3 plants/treatment, 10 vessels/plant).

Table 5
Immunodetection of the LM10 epitope specific for xylan in stem sections of *Cannabis sativa* (cv. Santhica 27). Plants were exposed for one week to Cd (20 µM) or Zn (100 µM) in the presence or in the absence of Si 2 mM. Mean ± Standard Deviation (SD). The different letters indicate that the values are significantly different from each other ($P < 0.05$; Tukey's HSD all-pairwise comparisons). Signal thickness (in µm) specify the thickness of the area wher signal was detected in the cell wall.

LM10							
Signal intensity						Signal thickness in cell wall (µm)	
Treatment	Epidermis	Collenchyma	Primary fibres	Secondary fibres	Xylem	Primary fibres	Secondary fibres
C	195 ± 57 *a*	123 ± 41 *ab*	411 ± 169 *a*	nd	27.12 ± 5.91 *b*	4.30 ± 2.47 *b*	nd
CSi	410 ± 93 *b*	172 ± 73 *bc*	313 ± 56 *a*	nd	29.78 ± 7.49 *b*	1.76 ± 0.23 *a*	nd
Cd	490 ± 159 *bc*	442 ± 181 d	717 ± 212 *b*	nd	12.66 ± 2.64 *a*	2.03 ± 0.56 *a*	nd
CdSi	666 ± 183 *c*	490 ± 192 *d*	715 ± 106 *b*	nd	14.90 ± 4.79 *a*	1.97 ± 0.48 *a*	nd
Zn	594 ± 258 *bc*	252 ± 76 *c*	411 ± 150 *a*	nd	20.20 ± 4.37 *ab*	2.10 ± 0.51 *a*	nd
ZnSi	258 ± 182 *a*	100 ± 71 *a*	345 ± 85 *a*	nd	21.78 ± 2.68 *ab*	1.80 ± 0.33 *a*	nd

Table 6
Immunodetection of the CBM3a epitope specific for crystalline cellulose in stem sections of *Cannabis sativa* (cv. Santhica 27). Plants were exposed for one week to Cd (20 µM) or Zn (100 µM) in the presence or in the absence of Si 2 mM. Mean (n = 3) ± Standard Deviation (SD). The different letters indicate that the values are significantly different from each other ($P < 0.05$; Tukey's HSD all-pairwise comparisons). Signal thickness (in µm) specify the thickness of the area wher signal was detected in the cell wall.

CBM3a							
Signal intensity						Signal thickness in cell wall (µm)	
Treatment	Epidermis	Collenchyma	Primary fibres	Secondary fibres	Xylem	Primary fibres	Secondary fibres
C	1009 ± 326 *a*	873 ± 370 *bc*	846 ± 280 *b*	862 ± 288 *b*	632 ± 136 *b*	2.54 ± 0.50 *b*	2.62 ± 0.66 *b*
CSi	778 ± 145 *a*	508 ± 72 *a*	507 ± 118 *a*	521 ± 96 *c*	449 ± 54 *a*	2.47 ± 0.41 *b*	2.37 ± 0.50 *ab*
Cd	753 ± 174 *a*	938 ± 149 *c*	1088 ± 263 *c*	nd	773 ± 132 *c*	1.95 ± 0.39 *a*	nd
CdSi	800 ± 196 *a*	859 ± 222 *bc*	1141 ± 196 *c*	669 ± 138 *a*	790 ± 150 *c*	2.49 ± 2.66 *a*	2.19 ± 0.40 *a*
Zn	786 ± 178 *a*	642 ± 153 *a*	915 ± 265 *bc*	720 ± 148 *ab*	653 ± 62 *b*	2.56 ± 0.38 *b*	2.21 ± 0.73 *a*
ZnSi	849 ± 130 *a*	678 ± 114 *ab*	1135 ± 267 *c*	724 ± 237 ab	717 ± 80 *bc*	2.49 ± 0.79 *b*	2.31 ± 0.51 *ab*

elongation and lignification through H_2O_2production modulation has been recently reviewed (Berni et al., 2018) : in cotton, Guo et al. (2016) observed that plants with downregulation of an ascorbate peroxidase (*GhAPX1AT*) are characterized by a significant increase in the number of fibres and by oxidative stress, which significantly reduces fibre elongation. During gene overexpression, cells show enhanced tolerance to oxidative stress suggesting that optimal levels of hydrogen peroxide are key mechanisms regulating fibre elongation (Guo et al., 2016). A high concentration of H_2O_2 would thus act as a signal for initiation of secondary wall thickening (Guo et al., 2016, Tang et al., 2014).

Peroxidases are necessary to initiate the polymerization of monolignols (Berthet et al., 2011; Chernova et al., 2018; Novo-Uzal et al., 2013). Our data show that in hemp stems, the expressions of PRX49 and PRX72, were higher under Cd/Zn treatment than in controls. Similarly, the abundance of PRX proteins increased (Fig. 8; PRX4 and PRX15 for Cd, PRX72 for Zn). Lignification occurs during normal growth but also during defense responses: in hemp stems, the increased lignin-related transcripts could be a strategy to reduce HM entry into the cell by making the CW less permeable. Besides their role in lignification, PRXs may have a role in gelatinous CW modification. In experiments conducted by Behr et al. (2018), S lignin staining and peroxidase activity were overlapping in bast fibres, and they observed higher abundances of both transcripts (orthologs of *AtPRX49*, *AtPRX52* and *AtPRX72*) and proteins (orthologs of AtPRX3, AtPRX52 and AtPRX54) at older stages of hemp development. Behr et al. (2019) also observed that in hemp, most of the signal of a peroxidase detected by the CsaPRX64 antibody had a distribution in the G-layer, with a scarcity or absence of signal in the S1-layer. The developing G-layer of phloem fibres from the tree *Mallotus japonicus* also shows a peroxidase activity, despite the absence of lignin (Nakagawa et al., 2014). The peroxidase activity detected in the G-layer may thus be involved in gelatinous CW modification, or in cellular defense mechanisms, and could be affected by plant exposure to Cd or Zn.

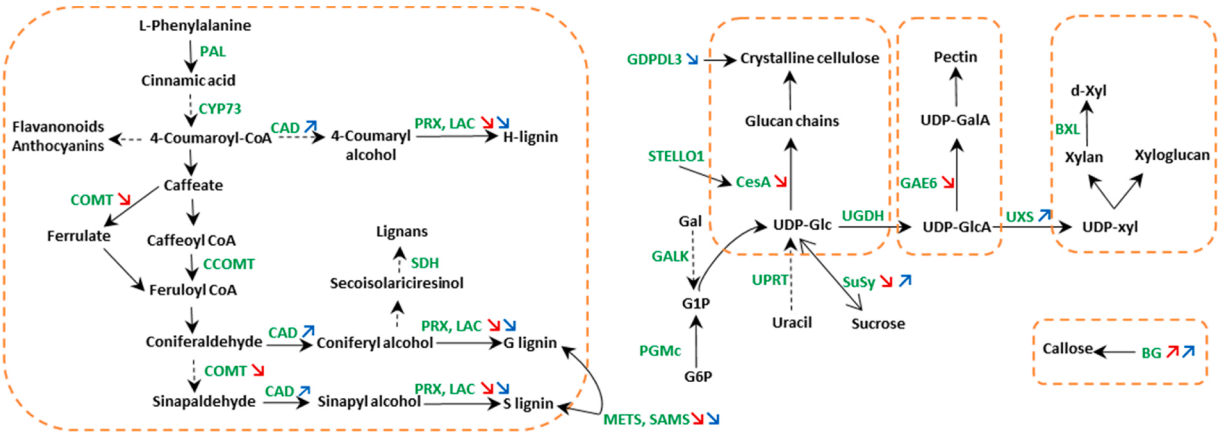

Fig. 8. Global overview of the impact of Cd and Zn on the abundance of proteins involved in the synthesis of cell wall precursors in hemp hypocotyls. Seedlings were exposed for one week either to Cd 20 µM, Zn 100 µM or Si 2 mM and proteins were extracted from hypocotyls. Colored arrows indicate a significant effect of Zn (in blue) or Cd (in red). The orange doted line delimits individual pathways.

Moreover, PRX72 participates in the biosynthesis of lignans, monolignol-derived molecules which may contribute to the hypo-lignification of bast fibres by subtracting monolignols from the lignin polymerization process (Behr, 2018). In lettuce and ryegrass, stem and root elongation is regulated by specific lignans, such as syringaresinol and sesamin (Yamauchi et al., 2015) and further experiments are thus required to precise the impact of Cd and Zn on lignan synthesis in hemp in relation to the observed root and shoot elongation decrease.

METS and SAMS are enzymes involved in the generation of methyl donors, required for G and S monolignol methylation (Behr et al., 2017; Shen et al., 2002; Tang et al., 2014). Their expression level decreased in the presence of Cd while a number of SAMS transcripts only slightly decreased in response to Zn excess. These genes are in general more expressed in the core tissue than in the cortical tissue (Guerriero et al., 2017b). Guerriero et al. (2017b) showed that the higher lignin content of the xylem tissues is correlated with an upregulation of the genes of the phenylpropanoid/monolignol pathway (*CAD, METS, SAMS, PAL*). We thus hypothesize that Cd-induced decrease in diameter and thickness of xylem vessels might be a consequence of METS and SAMS inhibition.

Xylan, the main hemicellulose of the SCW, was detected by LM10 antibody in xylem cells and the CW of primary bast fibres. In xylem cells, xylan is largely present in the lignifying SCW while in the bast fibres the G-layer is almost completely depleted in lignin and xylan (Behr, 2018). The chemical composition of xylan in these two tissues may be regulated to fulfil distinct functions, such as water conduction in xylem vessels and mechanical resistance in phloem fibres (Behr et al., 2019). The CW of primary bast fibres was more strongly labelled by the antibody in Cd-treated plants compared to control ones. In xylem vessels, only Zn exposure affected the signal intensity (higher). Considering that LM10 recognizes unsubstituted or low substituted xylan (McCartney et al., 2005), the results obtained suggest a decreased substitution of xylan in these CW, which may contribute to a higher CW stiffness caused by the HM (Shrestha et al., 2019). Chemical analyses will validate this hypothesis.

Pectin is considered as the main binding site for Cd. Structural changes frequently appear in the composition of pectic polysaccharide in plants exposed to Cd (Gutsch et al., 2019b). A variety of enzymes, including pectinesterase, β-like galactosidase, α-galactosidase are acting on the pectin network. This is especially the case for enhancement of pectin methylesterases (PME) which allow demethylesterification of homogalacturonan thus creating bing sites for Cd and avoiding its entry in cytosol (Hu et al., 2010; Gutsch et al., 2018). In Cd-treated plants, compared to control ones, the abundance of glucuronate 4-epimerase 6 (GAE6), involved in pectin synthesis, was decreased. We did not record any impact of heavy metals or Si treatment on PME abundance in our hemp samples. It has however to be mentioned that Zn excess triggered pectin acetylesterase accumulation. Pectin acetylesterase (E.C. 3.1.1.6; PAE) cleaves the acetylester bond from pectin, especially in homo-galacturonan where GalA residues can be acetylated at positions O-2 or O-3, also creating available binding sites for divalent cation binding.

It is concluded that Cd and Zn reduced bast fibre diameter in hemp and that Cd negatively affected lignin and cellulose synthesus while Zn had an opposite effect on cellulose. The two considered heavy metals had distinct effects on gene expression and specific protein synthesis. Silicon did not significantly improved plant growth on a short term basis but slightly decreased Cd content in roots and stems and had a specific impact on protein regulation in plants exposed to Cd stress.

Author's contributions

ML, GG and SL designed methodology; ML performed the whole experiment, treated and analyzed the data; AI contributed to mineral analysis and confocal microscopy; JFH and SL supervised the whole research process; ML and SL wrote the original draft; All authors reviewed the manuscript.

Declaration of Competing Interest

The authors report no declarations of interest.

Acknowledgements

This work was financed by ADEME (Agence de la Transition écologique; Convention MisChar n°1672C0044). The authors are grateful to Dr. C. Hachez and Mrs M.C. Eloy for assistance in using confocal microscope, to Dr P. Morsomme and Mr. H. Degand for their valuable help in proteomic analysis and to Mr. B. Capelle for his technical assistance during plant culture.

Appendix A. Supplementary data

Supplementary material related to this article can be found, in the online version, at doi:https://doi.org/10.1016/j.envexpbot.2020.104363.

References

Adrees, M., Ali, S., Rizwan, M., Zia-ur-Rehman, M., Ibrahim, M., Abbas, F., Farid, M., Qayyum, M.F., Irshad, M.K., 2015. Mechanisms of silicon-mediated alleviation of heavy metal toxicity in plants: a review. Ecotox. Environ. Saf. 119, 186–197.

Aiello, G., Fasoli, E., Boschin, G., Lammi, C., Zanoni, C., Citterio, A., Arnoldi, A., 2016. Proteomic characterization of hempseed (*Cannabis sativa* L.). J. Proteom. 147, 187–196.
Ali, H., Khan, E., Sajad, M.A., 2013. Phytoremediation of heavy metals – concepts and applications. Chemosphere 91, 869–881.
Andre, C.M., Hausman, J.F., Guerriero, G., 2016. *Cannabis sativa*: the plant of the thousand and one molecules. Front. Plant Sci. 7, 19.
Angelova, V., Ivanova, R., Delibaltova, V., Ivanov, K., 2004. Bio-accumulation and distribution of heavy metals in fibre crops (flax, cotton and hemp). Ind. Crops Prod. 19, 197–205.
Arru, L., Rognoni, S., Baroncini, M., Bonatti, P.M., Perata, P., 2004. Copper localization in *Cannabis sativa* L. grown in copper-rich solution. Euphytica 140, 33–38.
Behr, M., 2018. Molecular Investigation of Cell Wall Formation in Hemp Stem Tissues. PhD Thesis. Université catholique de Louvain, Louvain-la-Neuve, Belgium, p. 351.
Behr, M., Legay, S., Žižková, E., Motyka, V., Dobrev, P.I., Hausman, J.F., Lutts, S., Guerriero, G., 2016. Studying secondary growth and bast fiber development: the hemp hypocotyl peeks behind the wall. Front. Plant Sci. 7, 1733.
Behr, M., Legay, S., Hausman, J.F., Lutts, S., Guerriero, G., 2017. Molecular investigation of the stem snap point in textile hemp. Genes 8, 363.
Behr, M., Sergeant, K., Leclercq, C.C., Planchon, S., Guignard, C., Lenouvel, A., Renaut, J., Hausman, J.F., Lutts, S., Guerriero, G., 2018. Insights into the molecular regulation of monolignol-derived product biosynthesis in the growing hemp hypocotyl. BMC Plant Biol. 18, 1.
Behr, M., Faleri, C., Hausman, J.F., Planchon, S., Renaut, J., Cai, G., Guerriero, G., 2019. Distribution of cell-wall polysaccharides and proteins during growth of the hemp hypocotyl. Planta 250, 1539–1556.
Berni, R., Luyckx, M., Xu, X., Legay, S., Sergeant, K., Hausman, J.F., Lutts, S., Cai, G., Guerriero, G., 2018. Reactive oxygen species and heavy metal stress in plants: impact on the cell wall and secondary metabolism. Environ. Exp. Bot. 161, 98–106.
Berni, R., Mandlik, R., Hausman, J.F., Guerriero, G., 2020. Silicon-induced mitigatory effects in salt-stressed hemp leaves. Physiol. Plant. (in press).
Berthet, S., Demont-Caulet, N., Pollet, B., Bidzinski, P., Cézard, L., Le Bris, P., Borrega, N., Hervé, J., Blondet, E., Balzergue, S., Lapierre, C., Jouanin, L., 2011. Disruption of LACCASE4 and 17 results in tissue-specific alterations to lignification of *Arabidopsis thaliana* stems. Plant Cell 23, 1124–1137.
Bhat, J.A., Shivaraj, S.M., Singh, P., Navadagi, D.B., Tripathi, D.K., Dash, P.K., Solanke, A.U., Sonah, H., Deshmukh, R., 2019. Role of silicon in mitigation of heavy metal stresses in crop plants. Plants 8, 71.
Bona, E., Marsano, F., Cavaletto, M., Berta, G., 2007. Proteomic characterization of copper stress response in *Cannabis sativa* roots. Proteomics 7, 1121–1130.
Branda, F., Malucelli, G., Durante, M., Piccolo, A., Mazzei, P., Costantini, A., Silvestri, M., Pennetta, M., Bifulco, A., 2016. Silica treatment: a fire retardant strategy for hemp fabric/epoxy composites. Polymers 8, 131.
Candilo, M.D., Ranalli, P., Dal Re, L., 2004. Heavy metal tolerance and uptake of Cd, Pb and Tl by hemp. Adv. Hortic. Sci. 18, 138–144.
Chandra, R., Kang, H., 2016. Mixed heavy metal stress on photosynthesis, transpiration rate and chlorophyll content in poplar hybrids. For. Sci. Technol. 122, 55–61.
Chernova, T.E., Mikshina, P.V., Salnikov, V.V., Ibragimova, N.N., Sautkina, O.V., Gorshkova, T.A., 2018. Development of distinct cell wall layers both in primary and secondary phloem fibers of hemp (*Cannabis sativa* L.). Ind. Crops Prod. 117, 97–109.
Citterio, S., Santagostino, A., Fumagalli, P., Prato, N., Ranalli, P., Sgorbati, S., 2003. Heavy metal tolerance and accumulation of Cd, Cr and Ni by *Cannabis sativa* L. Plant Soil 256, 243–252.
Cosio, C., Dunand, C., 2008. Specific functions of individual class III peroxidase genes. J. Exp. Bot. 60, 391–408.
Dufey, I., Gheysens, S., Ingabire, A., Lutts, S., Bertin, P., 2014. Silicon application in cultivated rices (*Oryza sativa* L. and *Oryza glaberrima* Steud) alleviates iron toxicity symptoms through the reduction of iron concentration in the leaf tissue. J. Agron. Crop Sci. 200, 132–142.
Etesami, H., Jeong, B.R., 2018. Silicon (Si): review and future prospects on the action mechanisms in alleviating biotic and abiotic stresses in plants. Ecotox. Environ. Saf. 147, 881–896.
Feng, W., Guo, Z., Xiao, X., Peng, C., Shi, L., Ran, H., Xu, W., 2020. A dynamic model to evaluate the critical loads of heavy metals in agricultural soil. Ecotox. Environ. Saf. 197, 110607.
García-Tejero, L.F., Durán Zuazo, V.H., Sánchez-Carnenero, C., Hernández, A., Ferreiro-Vera, C., Casano, S., 2019. Seeking suitable agronomical practices for industrial hemp (*Cannabis sativa* L.) cultivation for biomedical applications. Ind. Crop Prod. 139, 111524.
Gorshkova, T.A., Sal'nikov, V.V., Chemikosova, S.B., Ageeva, M.V., Pavlencheva, N.V., Van Dam, J.E.G., 2003. The snap point: a transition point in *Linum usitatissimum* bas fiber development. Ind. Crops Prod. 18, 213–221.
Gorshkova, T., Brutch, N., Chabbert, B., Deyholos, M., Hayashi, T., Lev-Yadun, S., Mellerowicz, E.J., Morvan, C., Neutelings, G., Pilate, G., 2012. Plant fiber formation: state of the art, recent and expected progress, and open questions. Crit. Rev. Plant Sci. 31, 201–228.
Granot, D., Stein, O., 2019. An overview of sucrose synthases in plants. Front. Plant Sci. 10, 95.
Guerriero, G., Sergeant, K., Hausman, J.F., 2013. Integrated-omics: a powerful approach to understanding the heterogeneous lignification of fibre crops. Intern. J. Mol. Sci. 14, 10958–10978.
Guerriero, G., Behr, M., Legay, S., Mangeot-Peter, L., Zorzan, S., Ghoniem, M., Hausman, J.F., 2017a. Transcriptomic profiling of hemp bast fibres at different developmental stages. Sci. Rep. 7, 4961.
Guerriero, G., Mangeot-Peter, L., Legay, S., Behr, M., Lutts, S., Siddiqui, K.S., Hausman, J.F., 2017b. Identification of fasciclin-like arabinogalactan proteins in textile hemp (*Cannabis sativa* L.): in silico analyses and gene expression patterns in different tissues. BMC Genom. 18, 741.
Guerriero, G., Law, C., Stokes, I., Moore, K.L., Exley, C., 2018a. Rough and tough. How does silicic acid protect horsetail from fungal infection? J. Trace Elem. Med. Biol. 47, 45–52.
Guerriero, G., Stokes, I., Exley, C., 2018b. Is callose required for silicification in plants? Biol. Lett. 14, 20180338.
Guerriero, G., Deshmukh, R., Sonah, H., Sergeant, K., Hausmann, J.F., Lentzen, E., Valle, N., Siddiqui, K.S., Exley, C., 2019. Identification of the aquaporin gene family in *Cannabis sativa* and evidence for the accumulation of silicon in its tissues. Plant Sci. 287, 110167.
Guerriero, G., Stokes, I., Valle, N., Hausman, J.F., Exley, C., 2020. Visualising silicon in plants: histochemistry silica sculptures and elemental imaging. Cells 9, 1066.
Guo, K., Du, X., Tu, L., Tang, W., Wang, P., Wang, M., Liu, Z., Zhang, X., 2016. Fibre elongation requires normal redox homeostasis modulated by cytosolic ascorbate peroxidase in cotton (*Gossypium hirsutum*). J. Exp. Bot. 67, 3289–3301.
Gutsch, A., Keunen, E., Guerriero, G., Renaut, J., Cuypers, A., Hausman, J.F., Sergeant, K., 2018. Long-term cadmium exposure influences the abundance of proteins that impact the cell wall structure in *Medicago sativa* stems. Plant Biol. 20, 1023–1035.
Gutsch, A., Vandionant, S., Sergeant, K., Jozefczak, M., Vangronsveld, J., Hausman, J.F., Cuypers, A., 2019a. Systems biology of metal tolerance in plants: a case study on the effects of Cd exposure on two model plants. Plant Metallomics and Functional Omics. Springer, Cham, pp. 23–37.
Gutsch, A., Sergeant, K., Keunen, E., Guerriero, G., Renaut, J., Hausman, J.F., Cuypers, A., 2019b. Does long-term cadmium exposure influence the composition of pectic polysaccharides in the cell wall of *Medicago sativa* stems? BMC Plant Biol. 19, 271.
Hernandez-Gomez, M.C., Rydahl, M.G., Rogowski, A., Morland, C., Cartmell, A., Crouch, L., et al., 2015. Recognition of xyloglucan by the crystalline cellulose-binding site of a family 3a carbohydrate-binding module. FEBS Lett. 589, 2297–2303.
Herrero, J., Esteban-Carrasco, A., Zapata, J.M., 2013. Looking for *Arabidopsis thaliana* peroxidases involved in lignin biosynthesis. Plant Physiol. Biochem. 67, 77–86.
Hu, G., Huang, S., Chen, H., Wang, F., 2010. Binding of four heavy metals to hemicelluloses from rice bran. Food Res. Int. 43, 203–206.
Hussain, R., Weeden, H., Bogush, D., Deguchi, M., Soliman, M., Potlakayala, S., Katam, R., Goldman, S., Rudrabhatta, S., 2019a. Enhanced tolerance of industrial hemp (*Cannabis sativa* L.) plants on abandoned mine land soil leads to overexpression of cannabinoids. PLoS One 14, e0221570.
Hussain, A., Calabria-Holley, J., Lwarence, M., Ansell, M.P., Jiang, Y., Schorr, D., Blanchet, P., 2019b. Development of novel building composites based on hemp and multi-functional silica matrix. Composites B 156, 266–273.
Imtiaz, M., Rizwan, M.S., Mushtag, M.A., Ashraf, M., Shahazad, S.M., Yousaf, B., Saeed, D.A., Rizwan, M., Nawaz, M.A., Mehmood, S., Tu, S., 2016. Silicon occurrence, uptake, transport and mechanisms of heavy metals, minerals and salinity enhanced tolerance in plants with future prospects: a review. J. Environ. Manag. 183, 521–529.
Jaskulak, M., Grobela, A., Vandenbulcke, F., 2020. Modelling assisted phytoremediation of soils contaminated with heavy metals – main opportunities, limitations, decision making and future prospects. Chemosphere 249, 126196.
Jenkins, C., Orsburn, B., 2020. The Cannabis proteome draft map project. Int. J. Mol. Sci. 21, 965.
Jiang, Y., Bourebrab, M.A., Sid, N., Taylor, A., Collet, F., Pretot, S., Hussain, A., Ansell, M., Lawrence, M., 2018. Improvement of water resistance of hemp woody substrates through deposition of functionalized silica hydrophobic coating, while retaining excellent moisture buffering properties. Sustain. Chem. Eng. 6, 10151–11016.
Kumar, S., Singh, R., Kumar, V., Rani, A., Jain, R., 2017. *Cannabis sativa*: a plant suitable for phytoremediation and bioenergy production. Phytoremediation Potential of Bioenergy Plants. Springer, Singapore, pp. 269–285.
Lefèvre, I., Vogel-Mikuš, K., Jeromel, J., Vavpetič, P., Planchon, S., Arčon, I., T. van Elteren, J., Lepoint, G., Gobert, S., Renaut, J., Pelicon, P., Lutts, S., 2014. Cadmium and zinc distribution in relation to their physiological impact in the leaves of the accumulating *Zygophyllum fabago* L. Plant Cell Environ. 37, 1299–1320.
Lefèvre, I., Vogel-Mikuš, K., Arčon, I., Lutts, S., 2016. How do roots of the metal-resistant perennial bush *Zygophyllum fabago* cope with cadmium and zinc toxicities? Plant Soil 404, 193–207.
Linger, P., Müsig, J., Fischer, H., Kobert, J., 2002. Industrial hemp (*Cannabis sativa* L.) growing on heavy metal contaminated soil: fibre quality and phytoremediation potential. Ind. Crop Prod. 16, 33–42.
Loiacono, S., Crini, G., Martel, B., Chanet, G., Cosentino, C., Raschetti, M., Placet, V., Torri, g., Morin-Crini, N., 2017. Simultaneous removal of Cd, Co, Cu, Mn, Ni, and Zn from synthetic solutions on a hemp-based felt; II. Chemical modification. J. Appl. Polym. Sci. 45138.
Luyckx, M., Hausman, J.F., Lutts, S., Guerriero, G., 2017a. Silicon and plants: current knowledge and technological perspectives. Front. Plant Sci. 8, 411.
Luyckx, M., Hausman, J.F., Lutts, S., Guerriero, G., 2017b. Impact of silicon in plant biomass production: focus on bast fibres, hypotheses, and perspectives. Plants 6, 37.
Luyckx, M., Berni, R., Cai, G., Lutts, S., Guerriero, G., 2019. Impact of heavy metals on non-food herbaceous crops and prophylactic role of Si. Plant Metallomics and Functional Omics. Springer, Cham, pp. 303–321.
Mangeot-Peter, L., Legay, S., Hausman, J.F., Esposito, S., Guerriero, G., 2016. Identification of reference genes for RT-qPCR data normalization in *Cannabis sativa* stem tissues. Int. J. Mol. Sci. 17, 1556.

McCartney, L., Marcus, S.E., Knox, J.P., 2005. Monoclonal antibodies to plant cell wall xylans and arabinoxylans. J. Histochem. Cytochem. 53, 543–546.
Meers, E., Ruttens, A., Hopgood, M., Lesage, E., Tack, F.M.G., 2005. Potential of *Brassica rapa*, *Cannabis sativa*, *Helianthus annuus* and *Zea mays* for phytoextraction of heavy metals from calcareous dredged sediment derived soils. Chemosphere 61, 561–572.
Mihoc, M., Pop, G., Alexa, E., Radulov, I., 2012. Nutritive quality of romanian hemp varieties (*Cannabis sativa* L.) with special focus on oil and metal contents of seeds. Chem. Cent. J. 6, 122.
Mokshina, N., Gorshkov, O., Ibragimova, N., Chernova, T., Gorshkova, T., 2017. Cellulosic fibres of flax recruit both primary and secondary cell wall cellulose synthases during deposition of thick tertiary cell walls and in the course of graviresponse. Funct. Plant Biol. 44, 820–831.
Morin-Crini, N., Loiacono, S., Placet, V., Torri, G., Bradu, C., Kostić, M., Cosentino, C., Chanet, G., martel, B., Lichtfous, E., Crini, G., 2019. Hemp-based adsorbents for sequestration of metals: a review. Environ. Chem. Lett. 17, 393–408.
Nakagawa, K., Yoshinaga, A., Takabe, K., 2014. Xylan deposition and lignification in the multi-layered cell walls of phloem fibers in *Mallotus japonicus* (Euphorbiaceae). Tree Physiol. 34, 1018–1029.
Neumann, D., zur Nieden, U., 2001. Silicon and heavy metal tolerance of higher plants. Phytochemistry 56, 685–692.
Neutelings, G., 2011. Lignin variability in plant cell walls: contribution of new models. Plant Sci. 181, 379–386.
Novo-Uzal, E., Fernández-Pérez, F., Herrero, J., Gutiérrez, J., Gómez-Ros, L.V., Bernal, M.Á., Díaz, J., Cuello, J., Pomar, F., Pedreño, M.Á., 2013. From Zinnia to *Arabidopsis*: approaching the involvement of peroxidases in lignification. J. Exp. Bot. 64, 3499–3518.
O'Lexy, E., Kasai, K., Clarck, N., Fujiwara, T., Sozzani, R., Gallagher, K.L., 2018. Exposure to heavy metal stress triggers changes in plasmodesmatal permeability via deposition and breakdown of callose. J. Exp. Bot. 69, 3715–3728.
Pejic, B., Vukcevic, M., Kostic, M., Skundric, P., 2009. Biosorption of heavy metal ions from aqueous solutions by short hemp fibers: effect of chemical composition. J. Hazard. Mater. 164, 146–153.
Pietrini, F., Passatore, L., Patti, V., Francocci, F., Giovanozzi, A., Zacchini, M., 2019. Morpho-physiological and metal-accumulation responses of hemp plants (*Cannabis sativa* L.) grown on soil from an agro-industrial contaminated area. Water 11, 808.
Pogrzeba, M., Krzyżak, J., Rusinowski, S., McCalmont, J.P., Jensen, E., 2019. Energy crop at heavy metal-contaminated arable land as an alternative for food and feed production: biomass quantity and quality. Plant Metallomics and Functional Omics. Springer, Cham, pp. 1–21.
Seifikalhor, M., Aliniaeifard, S., Hassani, B., Niknam, V., Lastochkina, O., 2019. Diverse role of γ-aminobutyric acid in dynamic plant cell responses. Plant Cell Rep. 38, 1–21.
Sharma, S.S., Dietz, K.J., Mimura, T., 2016. Vacuolar compartmentalization as indispensable component of heavy metal detoxification in plants. Plant Cell Environ. 29, 1112–1126.
Shen, B., Li, C., Tarczynski, M.C., 2002. High free-methionine and decreased lignin content result from a mutation in the *Arabidopsis* S-adenosyl-L-methionine synthetase 3 gene. Plant J. 29, 371–380.
Shrestha, U.R., Smith, S., Pingali, S.V., Yang, H., Zahran, M., Breunig, L., et al., 2019. Arabinose substitution effect on xylan rigidity and self-aggregation. Cellulose 26, 2267–2278.
Stevulova, N., Cigasova, J., Estokova, A., Terpakova, E., Geffert, A., Kacik, F., Singovszka, E., Holub, M., 2014. Properties and characterization of chemically modified hemp hurds. Materials 7, 8131–8150.
Tang, H.M., Liu, S., Hill-Skinner, S., Wu, W., Reed, D., Yeh, C.T., Nettleton, D., Schnable, P.S., 2014. The maize brown midrib2 (bm2) gene encodes a methylenetetrahydrofolate reductase that contributes to lignin accumulation. Plant J. 77, 380–392.
Taylor, N.G., Howells, R.M., Huttly, A.K., Vickers, K., Turner, S.R., 2003. Interactions among three distinct CesA proteins essential for cellulose synthesis. Proc. Nat. Acad. Sci. 100, 1450–1455.
Vareda, J.P., Valente, A.J.M., Durães, L., 2019. Assessment of heavy metal pollution from anthropogenic activities and remediation strategies. J. Environ. Manag. 246, 101–118.
Vincent, D., Binos, S., Rochfort, S., Spangenberg, G., 2019. Top-down proteomics of medicinal cannabis. Proteomes 7, 33.
Vukcevic, M., Pejic, B., Lausevic, M., Pajic-Lijakovic, I., Kostic, M., 2014. Influence of chemically modified short hemp fiber structure on biosorption process of Zn^{2+} ions from waste water. Fib. Pol. 15, 687–697.
Wessel, D., Flügge, U.I., 1984. A method for the quantitative recovery of protein in dilute solution in the presence of detergents and lipids. Anal. Biochem. 138, 141–143.
Wu, J.W., Shi, Y., Zhu, Y.X., Wang, Y.C., Gong, H.J., 2013. Mechanisms of enhanced heavy metal tolerance in plants by silicon: a review. Pedosphere 23, 815–825.
Yamauchi, S., Ichikawa, H., Nishiwaki, H., Shuto, Y., 2015. Evaluation of plant growth regulatory activity of furofuran lignan bearing a 7, 9′: 7′, 9-diepoxy structure using optically pure (+)-and (−)-enantiomers. J. Agric. Food Chem. 63, 5224–5228.